A REPRINT FROM THE JANUARY 1995 ISSUE OF

PROCESS SAFETY PROGRESS

AN ADVANCED METHOD FOR THE ESTIMATION OF REACTION KINETICS, SCALEUP, AND PRESSURE RELIEF DESIGN

G. A. Melhem
Arthur D. Little Inc.
Cambridge, MA 02140

H. G. Fisher
Union Carbide Corp.
South Charleston, WV 25303

D. A. Shaw
Monsanto Co.
St. Louis, MO 63167

An Advanced Method for the Estimation of Reaction Kinetics, Scaleup, and Pressure Relief Design

G. A. Melhem
Arthur D. Little Inc., Cambridge, MA 02140

H. G. Fisher
Union Carbide Corp., South Charleston, WV 25303

and

D. A. Shaw
Monsanto Co., St. Louis, MO 63167

This paper presents an advanced modeling approach which significantly improves predictions of reaction rates and critical data that engineers need to design effective pressure relief systems. Ideally, pressure relief systems are sized exactly for the reaction characteristics of the chemicals in the vessel. However, with many chemicals and chemical mixtures, reaction chemistry is difficult to characterize because the individual components interact in complex ways. Furthermore, the high cost and risk of full-scale reactivity experiments make test data scarce. Chemical engineers bridge this gap in part with small-scale tests and modeling computer codes such as the one developed by the Design Institute for Emergency Relief Systems (DIERS). The comprehensive approach developed in this paper provides a reliable design basis for difficult systems, including highly energetic and nonideal reactions, systems with continuing reactions in piping and containment vessels, and systems where homogeneous bubble collapse caused by rapid depressurization could cause a catastrophic vessel failure. We first examine possible mechanisms for catastrophic vessel failure and associated consequences. Next, we outline a detailed approach for emergency relief system design and reactivity testing.

THERMODYNAMIC ANALYSIS

Vessel rupture is caused by an increase in the internal energy of the contents and insufficient emergency relief. When a vessel ruptures, the internal energy of the contents provides a source of fragmentation/deformation energy for the shell, kinetic energy imparted to contents and fragments, and blast wave energy. Clearly, this process is not reversible as some internal energy will be dissipated as turbulence and heat transferred to the surroundings. Under external heating by fire or internal heating by a runaway reaction or both, the temperature of the tank walls increases, the yield and tensile strength of the vessel walls decrease, and resistance to internal pressure decreases as well.

Upon vessel failure, the superheated liquid exhibits a sudden pressure drop to ambient pressure. To achieve equilibrium, internal energy stored in the liquid as superheat vaporizes a fraction of the liquid, i.e., the liquid will flash. The rapid vapor bubble growth causes the remaining liquid to break up into small droplets. Depending on the available energy content, a fraction of the droplets is entrained into the vapor cloud as an aerosol while the remainder rains out.

Rapid depressurization of a vessel can lead to explosive boiling of the liquid contents. Depressurization can be attributed to flow and/or expansion. The same phenomenon, i.e., explosive boiling of liquids, can be induced by rapid heating of the liquid and is sometimes referred to as rapid phase transitions. As shown in Figure 1, the pressure will drop below the saturation point following rapid depressurization. The rate of pressure drop influences this pressure undershoot which in turn influences the superheat available for bubble nucleation. Large depressurization rates can lead to large undershoots and thus bubble nucleation superheats. The pressure will recover when the pressure rise caused by bubble generation is equal to the rate of imposed pressure drop at flashing inception. If the rate

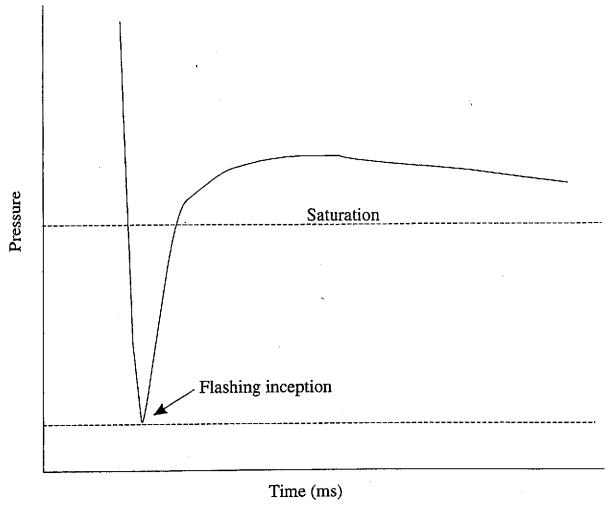

FIGURE 1. Flashing inception following a sudden pressure drop.

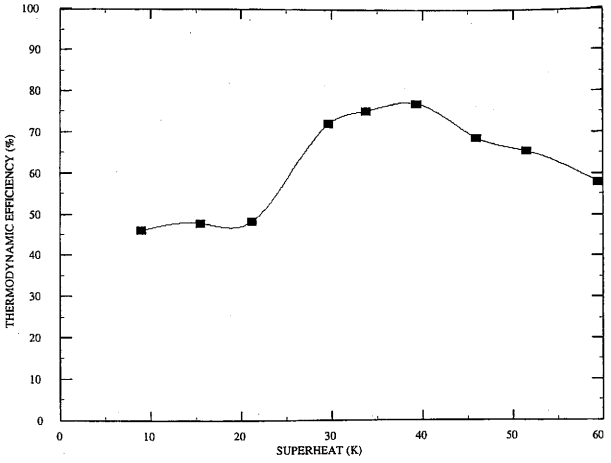

FIGURE 2. Fraction of available energy converted into kinetic energy.

of pressure drop is large enough, a metastable liquid can form upon depressurization. A sharp pressure rise caused by spontaneous bubble generation follows. One should note that rapid depressurization rates can render heterogeneous bubble nucleation sites inactive. As the internal temperature/pressure reach the superheat limit, depressurization rates required to cause a metastable liquid to form become smaller. If we assume that the vessel contents undergo isentropic expansion, we can calculate the total amount of available energy stored in the superheated liquid and/or the vapor. The amount of available energy is the difference between the initial internal energy content of the vessel before failure and the final internal energy contents of the resulting vapor-liquid mixture (under equilibrium) minus the PV work done on the atmosphere due to volumetric expansion (blast wave energy). If we were to convert all available internal energy into kinetic energy imparted to the vessel contents, we obtain the following relation:

$$A_E=\frac{1}{2}u^2=\frac{U_0}{M_{w_0}}-Y_S\frac{U_{1,v}}{M_{w_{1,v}}}-(1-Y_S)\frac{U_{1,l}}{M_{w_{1,l}}}-P_s(v_1-v_0) \quad (1)$$

A similar expression can be derived as a function of enthalpy:

$$\frac{1}{2}u^2=\frac{H_{0,l}}{M_{w_0}}-Y_S\frac{H_{1,v}}{M_{w_{1,v}}}-(1-Y_S)\frac{H_{1,l}}{M_{w_{1,l}}}-v_0(P_0-P_s) \quad (2)$$

Nolan *et al.* [*1*] (also see Bettis *et al.* [*2*]) conducted small-scale experimental work where they simulated sudden vessel failure. They used a spherical glass vessel. The fluids used were refrigerant 11 and refrigerant 114. Sudden failure was simulated by destruction of the glass vessel.

Table 1 shows a summary of experimental expansion velocities reported by Nolan *et al.* for varying storage pressures ata 50 percent fill level. The experimental values are compared to predicted values based on equation (1). Converting all available energy into kinetic energy should lead to an overestimate of the velocity term. This is shown by Table 1. As noted earlier, a part of the vessel energy is dissipated as turbulence, kinetic energy imparted to vessel fragments, vaporization, etc. We can, however, calculate from the measured values of expansion velocities an equivalent amount of available energy. We define thermodynamic efficiency (E) as the ratio of measured available energy to the calculated theoretical value:

$$E=\frac{A_{E_{\text{actual}}}}{A_{E_{\text{theory}}}} \quad (3)$$

Figure 2 plots E as a function of storage superheat (actual storage temperature—boiling point at 101325 Pa) for the data reported in Table 1. An average of 62 percent of available energy is converted into kinetic energy.

BOILING LIQUID EXPANDING VAPOR EXPLOSIONS

A Boiling Liquid Expanding Vapor Explosion (BLEVE) is the violent rupture of a pressure vessel containing saturated liquid/vapor at a temperature well above its atmospheric boiling point. The resulting flash evaporation of a large fraction of the liquid produces a large vapor cloud. If the vapor is flammable and if an ignition source is present at the time of vessel rupture, the vapor cloud burns in the form of a large rising fireball [*3*].

For pure materials, it is fairly straightforward to determine

Table 1 Expansion Velocities for Refrigerant 11 from Simulated Catastrophic Vessel Failures

T_0 (K)	P_0 (kPa)	$\rho_{v,0}$ (kg/m^3)	$\rho_{l,0}$ (kg/m^3)	$Y_{S,0}$	u_{actual} (m/s)	A_E (J/kg)	$Y_{S,1}$	u_{theory} (m/s)
306.0	140	7.87	1458	0.0054	11	132	0.050	16.2
312.5	172	9.59	1442	0.0066	19	378	0.082	27.4
318.3	206	11.35	1428	0.0078	26	703	0.110	37.4
326.7	264	14.32	1407	0.0100	44	1347	0.151	51.9
330.8	296	15.97	1396	0.0113	51	1734	0.171	58.9
336.4	345	18.47	1381	0.0131	60	2343	0.197	68.0
343.0	410	21.80	1364	0.0157	66	3175	0.230	79.0
348.5	471	24.90	1349	0.0180	72	3961	0.255	89.0
356.5	570	30.04	1326	0.0220	78	5260	0.293	102.5

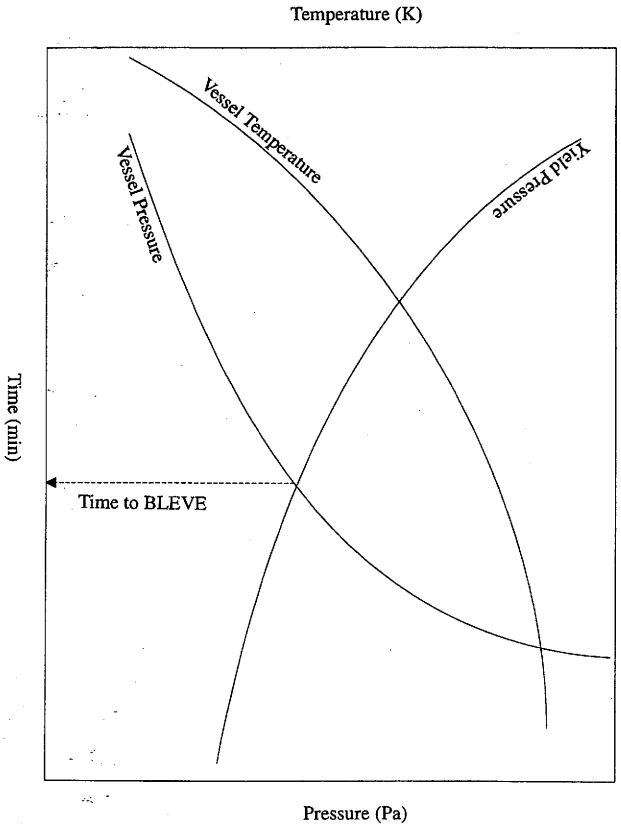

FIGURE 3. Time to BLEVE.

whether the saturated contents are significantly above the normal boiling point, i.e., the degree of superheat. Mixtures do not have a well defined normal boiling point, but rather are characterized by a range of temperatures over which boiling occurs. This temperature range is bounded between the bubble point and the dew point. The bubble point is the state at which the first vapor bubble starts to form. The dew point is the state at which the first drop of liquid starts to form.

In a BLEVE scenario, a violent rupture occurs because significant overpressure builds up as the vessel wall weakens, both resulting from the heating by the external fire exposure or by a chemical reaction (see Figure 3). Pressure builds up because of energy addition to the vessel contents and/or the addition of mass to the vapor space caused by liquid boiling. Fire exposure can range from full vessel engulfment to localized flame impingement. Historically, the majority of accidents where BLEVEs occurred involved flammable liquids such as propane and butane. The ignition resulting in a fireball was caused by a surrounding fire. Reported BLEVEs are summarized in reference [*4*].

During the last two decades, experimental research efforts have been focused on providing a better understanding of BLEVEs under external fire impingement conditions. BLEVE hazards caused by thermal ruptures (fire exposure) tend to be more severe than those caused by other means such as mechanical damage or overfilling.

A comprehensive summary of BLEVEs under fire impingement is given by Leslie and Birk [*5*]. Their summary covers experimental work as well as computer models, BLEVE theories, projectile modeling, blast and missile effects, and case studies, and includes work done by Roberts *et al.* [*6*], Moodie *et al.* [*7*], Droste and Schoen [*8*], Schoen and Droste [*9*], and many others.

VESSEL FAILURE MECHANISMS

There are two possible mechanisms which can lead to catastrophic vessel failure upon rapid depressurization which is typically caused by metal failure or relief device actuation:

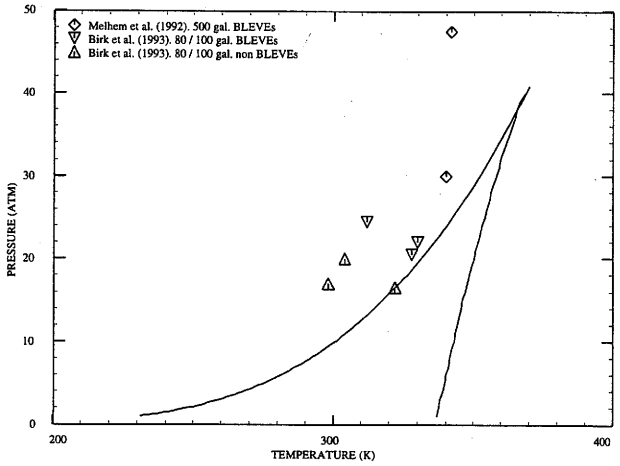

FIGURE 4. Mechanical stability limit for propane.

- Spontaneous nucleation at the thermodynamic stability limit, i.e. the superheat limit.
- Cavitation caused by homogeneous nucleation at temperatures lower than the superheat limit.

The superheat limit was first proposed in the late 70s as a possible mechanism for explaining catastrophic vessel failures. Reid [*10*], Jones [*11*], Martinsen *et al.* [*12*], Davenport [*13*], and Dunn [*14*] suggest that BLEVEs are superheat explosions and therefore are easily predicted by assessing the superheat limit for any pressurized liquid material.

The superheat limit can be estimated using thermodynamics as a function of pressure, temperature and composition. For a pure component, the superheat limit is calculated as the temperature at which the pressure derivative with respect to total volume vanishes:

$$\frac{\partial P}{\partial V}=0 \tag{4}$$

Figures 4 and 5 illustrate the mechanical stability limit for propane and water. Equation 4 is calculated using an equation of state. For a mixture, however, thermodynamic stability is more complex and requires the use of an equation of state with analytic derivatives for the chemical potential. For example, for a three component mixture, this is given by (see [*15*, *16*, and *17*]):

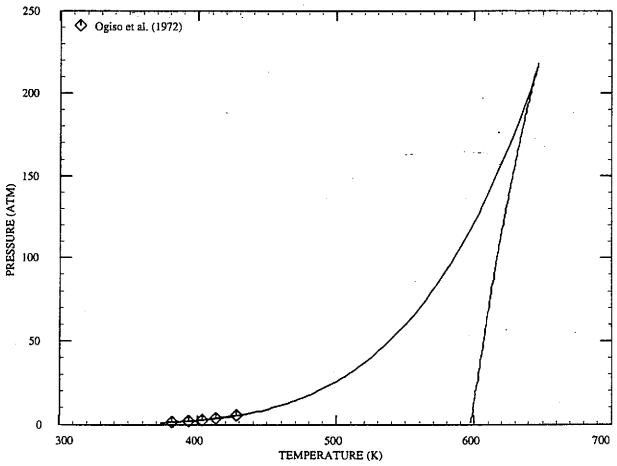

FIGURE 5. Mechanical stability limit for water.

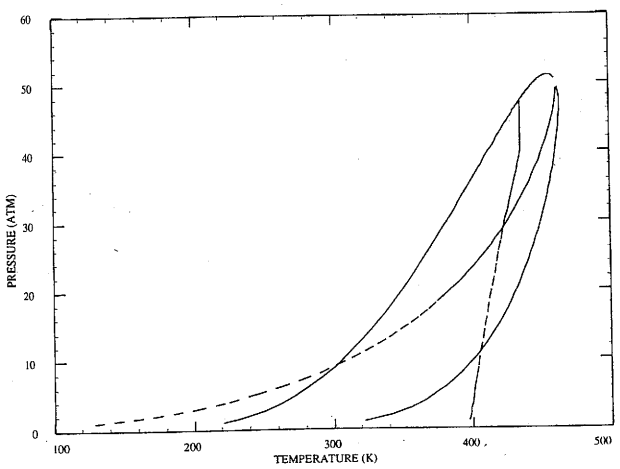

FIGURE 6. Mechanical stability limit for a mixture of ethane-propane-hexane.

$$\det\begin{bmatrix} \frac{\partial \mu_0}{\partial N_0} & \frac{\partial \mu_0}{\partial N_1} \\ \frac{\partial \mu_1}{\partial N_0} & \frac{\partial \mu_1}{\partial N_1} \end{bmatrix} = 0 \qquad (5)$$

Figure 6 illustrates the stability limits for a mixture of ethane, propane and hexane with corresponding mole fractions of 1/6, 1/3, and 1/2. Both the bubble point and dew point stability limits are shown in Figure 6. The superheat limit failure mechanism is schematically illustrated in Figure 7 and involves the following steps:

1. Rapid isentropic pressure drop (less than 1 s) across the stability limit causing the liquid to become metastable and superheated.
2. Spontaneous generation of bubbles (less than 1 microsecond) leading to large volumes of vapor.
3. Compression of the vapor leading to a very fast pressure rise. This is highly influenced by the vessel void fraction or fill level. Smaller vessel void fractions (higher fill levels) will lead to higher levels of pressure.

Catastrophic vessel failures have been reported at temperatures lower than the superheat limit as shown by Figures 4 and 5 for propane and water. These experiments were conducted by three different investigators (see Melhem *et al.* [*18*],

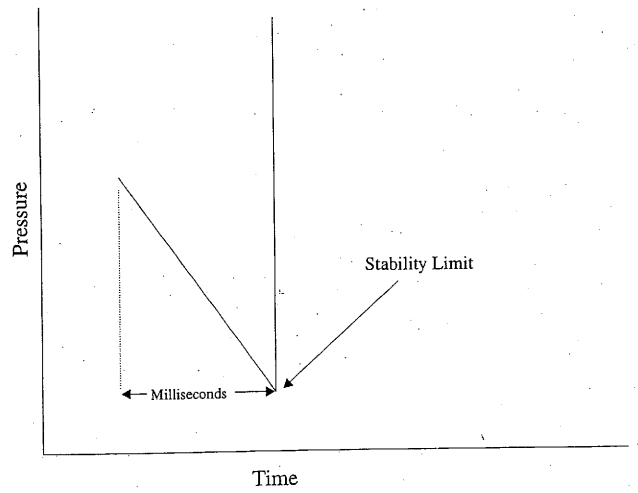

FIGURE 7. Superheat limit induced catastrophic vessel failure.

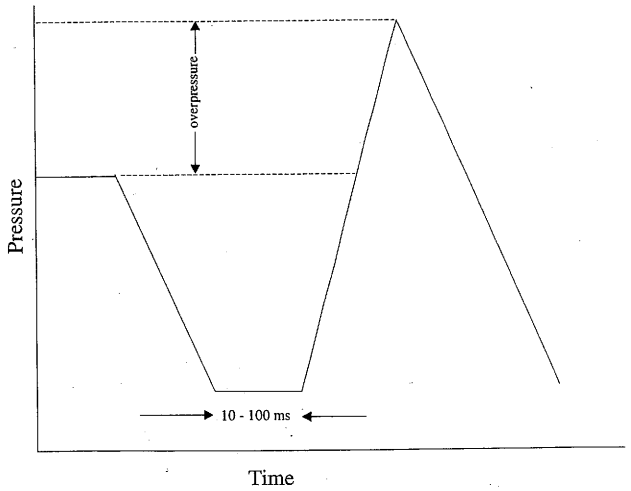

FIGURE 8. Cavitation induced catastrophic vessel failure.

Birk *et al.* [*19*] and Ogiso *et al.* [*20*]) and clearly show that vessel failures have occurred at small superheats. These failures can be attributed to very large rates of pressure drop leading to a metastable liquid and subsequent cavitation at temperatures below the superheat limit (see Venart [*21*]):

1. Rapid pressure drop (less than 1 s) causes the liquid to become metastable and superheated.
2. Due to the fast rate of pressure drop, heterogeneous nucleation sites become ineffective and the liquid become homogeneously nucleated as the final pressure is reached.
3. This is followed by homogeneous bubble generation and a rapid two-phase swell.
4. The flow through the rupture disk becomes choked and the vessel contents are repressurized.
5. Repressurization causes the coherent collapse of the newly formed bubbles. Liquid rushes in as the bubble collapse. As a result, the shock wave radiated throughout the liquid causes vessel failure [*22*].

The mechanism is illustrated in Figure 8. The rate of pressure drop required to cause liquid metastability will decrease as the critical temperature is approached [*23*]. A key variable to consider in pressure relief design is the rate of pressure decrease induced by rupture disk or relief device actuation. Ogiso *et al.* [*20*] conducted small-scale experiments with superheated water to investigate the impact of large rates of pressure drop on repressurization. Table 2 illustrates the impact of having a large rupture disk (i.e., large rates of pressure drop) on vessel repressurization.

An oversized rupture disk may not necessarily be safer depending on where the temperature that corresponds to the

Table 2 Impact of Rupture Disk Size on Vessel Repressurization for Water at 130 C*

Hole Diameter (mm)	Relative Diameter (Hole/Vessel)	Relative Area (Hole/Vessel)	Observation
50	1	1	Cavitation and overpressure
37.5	3/4	1/2	
25.0	1/2	1/4	
12.5	1/4	1/16	
6.7	1/7	1/56	Overpressure
3.2	1/16	1/244	No overpressure

*Data taken from Ogiso *et al.* (1972).

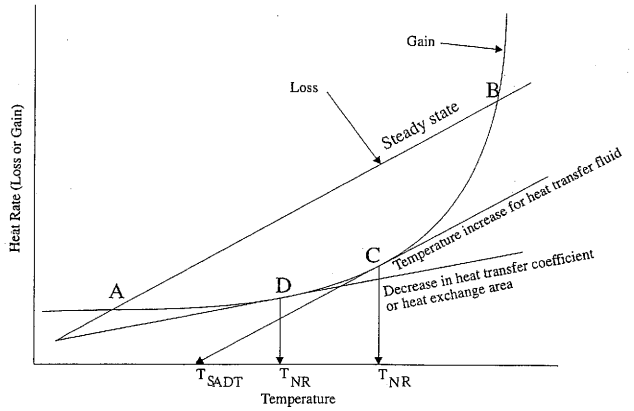

FIGURE 9. Thermal runaway due to high temperature.

rupture disk set pressure is on the stability curve. This temperature should not be allowed to exceed the superheat limit [*10*]. For reacting mixtures the superheat limit needs to be assessed for the mixture composition present in the vessel at the time of the relief device actuation. Relief systems should be designed to prevent rapid pressure decays.

THERMAL RUNAWAY/EXPLOSION

Catastrophic vessel failures can also be attributed to runaway exothermic reactions and/or reactions that generate gaseous products. As the temperature of the vessel contents deviates from safe operating bounds and becomes too high, the rate of heat production by the reaction exceeds the rate of heat loss and/or cooling capacity. While the reaction rate is an exponential function of temperature, the cooling capacity is only a linear function of temperature:

$$\frac{dQ_{rxn}}{dt} = V\Delta H_{rxn} K_0 \exp\left(-\frac{E}{R_g T}\right) C^n \qquad (6)$$

$$\frac{dQ_{\text{lost}}}{dt} = hA\,(T - T_s) \qquad (7)$$

Possible deviations that can lead to loss of temperature control include the decrease of the heat exchange coefficient h, decrease of the heat exchange area A and a high temperature for the heat exchange fluid T_s.

We consider first the case of steady state operation as shown in Figure 9. At steady state, the rate of heat generation equals the rate of heat removal. This is represented by points A and B in Figure 9. Point B is metastable. If the system temperature drops slightly, the rate of heat loss exceeds the rate of heat generation and the system steady state is driven to point A. If cooling capacity is lost, steady state can be restored if cooling is restored before the reaction temperature exceeds that at point B.

We next consider a high reaction temperature that is induced by an increase of the heating fluid temperature. Point C on Figure 9 is a limit temperature above which the heat rate produced by the reaction is larger than the heat removal rate. Above the temperature at point C, the system temperature increases steadily, causing the reaction rate to accelerate exponentially. The temperature at point C (where the slope of the heat generation line equals that of the heat loss line) is referred to as the temperature of no return. However, we should note that if cooling is restored before the temperature exceeds that at point B, steady state operation can be restored.

A high reaction temperature caused by partial loss of heat exchange coefficient or area is also represented in Figure 9. If the reaction temperature exceeds T_D, the system cannot be restored to steady state and will runaway. Heat loss to the surroundings is essential to the safety of any spontaneously decomposing solution. Interference with natural convection for example by adding insulation or changing from an uninsulated to an insulated vessel might also lead to a hazardous condition.

Other pathways that can lead reaction runaway include:

- Operational Error: The erroneous introduction/omission of reactant and/or catalyst which cause a reaction to accelerate at its normal operating temperature. Another good example is that of introducing an incompatible reactant to the vessel contents such that the reaction is immediately fast at the existing temperature of the contents.
- Hot Spots, i.e. high localized temperatures: This can be caused by the failure of agitation where the system fails to maintain a homogeneous temperature below certain onset limits. High localized temperatures can initiate a fast propagating reaction.
- Reactant Accumulation: This can arise in semibatch processes where the reaction is controlled by slow introduction of a specified reactant. At low reaction temperatures, the rate of consumption of reactant is less than the addition rate. As a result, the reactant accumulates in the reactor vessel. Afterwards, a small increase in temperature and/or the higher concentration of reactant initiates a runaway reaction.
- Segregation: Here, the reaction mixture splits into separate phases, where one or more phases are unstable. For example, liquid phases can split due to loss of mixing. Crystallization can occur due to cooling and lead to deposits of unstable solids on the reactor walls.
- Equipment failure: The failure of a feed pump might result in hazardous misproportionation or in slow flow through a heater leading to overheating.
- External Heating/Fire: This can lead to highly accelerated reaction rates because onset temperature is reached with less reactant consumption.
- Extended Residence Time: This is most frequent for autocatalytic reactions after an extended reaction/cycle time. An autocatalytic reaction produces its own catalyst or one of its controlling reactants after an induction time at constant temperature. Another example is monomer exhaustion of inhibitor which can occur during extended processing or storage.
- Spontaneous decomposition: This can be caused by preferential boiloff of a solvent in an unstable material solution. When the mixture is exposed to a fire or other heating sources, the light material preferentially boils off leaving a highly concentrated solution of an unstable material. The unstable material could reach temperatures leading to spontaneous autodecomposition.
- Spontaneous bubble collapse: This could cause autodecomposition for materials such as nitromethane. Compression waves leading to spontaneous collapse of bubbles can lead to local temperatures in excess of the autodecomposition limit. There have been reported accidents where a fast valve closure caused a shock wave resulting in compression and autodecomposition of a vapor nitromethane stream. Use of delayed timing to close valves is a good remedy for this cause.

EXTERNAL FIRE LOADING

For vessels containing nonreactive chemicals, fire exposure can increase the rate of energy/pressure accumulation due to:

- generation of vapor induced by liquid boiling-off and
- thermal expansion of vapor.

For vessels containing reactive chemicals the rate of energy/pressure accumulation is significantly increased because the

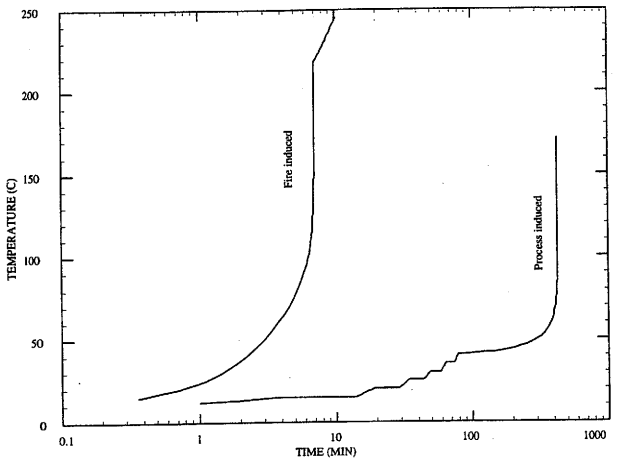

FIGURE 10. Impact of fire on temperature history for vessel containing hydrogen peroxide.

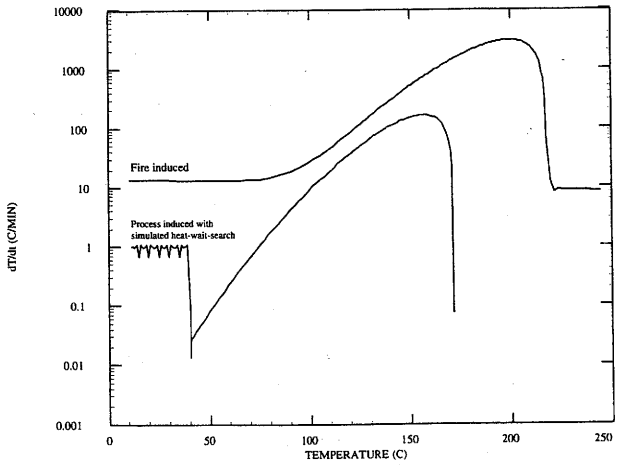

FIGURE 12. Impact of fire on reaction rates for a vessel containing hydrogen peroxide.

reaction temperature reaches onset with less reactant consumption. The effect of fire on reaction rates is highly nonlinear.

To illustrate this highly nonlinear effect of fire loading on vessel temperature and pressure behavior we consider a steel storage vessel containing a hydrogen peroxide/water solution that is exposed to an external heat flux of 100 kW/m^2. The vessel volume is 1 m^3 and the vessel metal mass is 500 kg. The peroxide/water solution consists of 159 kg of hydrogen peroxide and 716 kgs of water. The vessel initial temperature and pressure are 10 C and 1 bar respectively. Hydrogen peroxide decomposes in the liquid phase and forms oxygen and water according to the following stoichiometry:

$$H_2O_2 \rightarrow \frac{1}{2}O_2 + H_2O \tag{8}$$

The reaction is first order and has a temperature dependent rate described by the following expression

$$K = 1.5 \times 10^{12} \exp\left(-\frac{12{,}832}{T}\right) \tag{9}$$

where K is in s^{-1} and T is in Kelvins.

Figure 10 shows the simulated impact of fire on the temperature history (left curve) versus a process upset induced decomposition which is simulated using step heating to the onset at 0.02 C/min (right curve). The hydrogen peroxide decomposition was completed in seven minutes under fire exposure and in 420 minutes without fire exposure. The same can also be seen in Figure 11 for pressure.

Figure 12 illustrates the impact of fire on the peroxide decomposition rate. For the simulated process upset, a peak temperature rise rate of 160 C/min is reached while for the simulated fire exposure case a peak temperature rise rate of 2960 C/min is reached. The temperature rise rate attributed to fire exposure is 13 C/min as shown in Figure 10 for temperature below 45 C. The effect of external heating on reaction rates is significant for emergency relief system design.

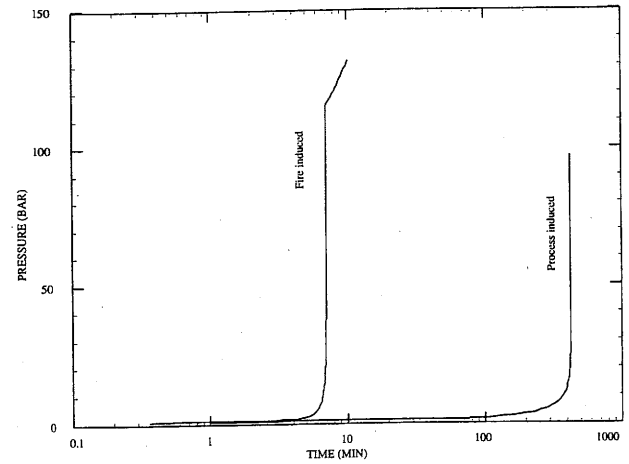

FIGURE 11. Impact of fire on pressure history for vessel containing hydrogen peroxide.

EXISTING STANDARDS

NFPA 30 [*24*] recommends that the fire exposure heat flux to a vessel be calculated using the following relations

$$q = 63\delta \text{ For } A_w < 18.6 \tag{10}$$

$$q = 224\delta A_w^{-0.434} \text{ For } 18.6 \le A_w < 93 \tag{11}$$

$$q = 612\delta A_w^{-0.662} \text{ For } 93 \le A_w < 260 \tag{12}$$

$$q = 4129\delta A_w^{-1} \text{ For } A_w \ge 260 \tag{13}$$

where q is the absorbed heat flux in kW/m^2, A_w is the vessel wetted surface area in m^2 and δ is a mitigation/environmental factor. The wetted area exponent recognizes that large vessels are less likely to be completely engulfed in an open fire than small vessels.

For sufficient drainage and for tanks with over 18.6 m^2 of wetted surface area, $\delta = 0.5$. For water spray systems in accordance with NFPA 15 [*25*], $\delta = 0.3$. For adequate insulation, $\delta = 0.3$. For water spray and insulation, $\delta = 0.15$. Only one δ value should be used per vessel. Also, the use of a δ value less than one must be checked against specific requirements for drainage, water spray, and insulation as outlined in NFPA 30.

A_w is calculated on the basis of 55% of the total exposed surface area of a sphere or spheroid, 75% of the total exposed surface area of a horizontal tank and the first nine meters above grade of the exposed shell of a vertical vessel.

The standard recommends that for vessels designed for pressures in excess of 108.22 kPa (3 psig) and with wetted surface areas exceeding 260 m^2, the absorbed heat flux should be obtained from:

$$q = 43.17\delta A_w^{-0.18} \text{ For } A_w \ge 260 \tag{14}$$

API 520 [*26*] recommends that equation (14) be applied for all values of A_w. Guidelines similar to those in NFPA 30 are provided by API 520 for the calculation of A_w and the mitigation/environment factor.

PRESSURE RELIEF DESIGN

The major of relief systems designed for process vessels can be divided into three categories:

A single-phase flow, nonreactive,
B two-phase flow, nonreactive, and
C single/two-phase flow due to runaway reaction or decomposition.

Designing relief systems for single-phase flow including liquid and vapor is straight forward. Existing national standards such as the ASME code section VIII, API 520, or NFPA 30 are typically used.

Relief system design for nonreactive systems which exhibit two-phase flow because of their foamy nature or because the vessel hydrodynamics should consider the effect of two-phase flow on vent size. A vent sized for vapor flow will not be adequate if two-phase flow is vented. DIERS has published extensively on vent sizing techniques for systems exhibiting two-phase flow. The details of these methods are well documented by the various DIERS publications and will not be described in this work [*27*, *28*, *29*, *30*, *31* and *32*].

DIERS methodology is also used to evaluate emergency relief requirements for reactive systems. This consists of three major steps:

1. Identify a design basis upset condition, i.e. worst credible scenario. This should also include vessel temperature, pressure, charge, chemical composition, and geometry.
2. Evaluate system characterization data for step 1 using physical chemistry testing. This includes physical properties for pure components and mixtures.
3. Evaluate the required vent area on the basis of steps 1 and 2 using formulas or computer codes which address liquid, gas, and two-phase flow.

The design basis upset condition is most important. For vessels where reactive chemicals are stored or processed, typical upset conditions include:

1. loss of cooling,
2. loss of agitation,
3. contamination, and
4. external fire.

A reactive event caused by external fire, should account for vessel insulation, a glass lining, jacketing or protection by water spray. In these situations heat transfer to the vessel contents is limited. In addition, fire durations should be selected based on available flammable inventory on site.

For reactive systems, essential parameters that should be evaluated include:

1. System Thermal Stability, i.e. nature and relative magnitude of any exothermic (or endothermic) effects. These include primary thermal runaway and any subsequent secondary decomposition reactions.
2. Total Heat Release, characterized by the specific reaction heat release per (mass or molar) unit of reacting material.
3. Rate of Heat Release, characterized by global kinetic parameters describing heat generation as a function of temperature and residual reactant concentration.
4. Rate of Gas Generation, due to volatilization of liquid components and vapor expansion effects with increasing reaction temperature or generation of additional gaseous reaction or decomposition products.

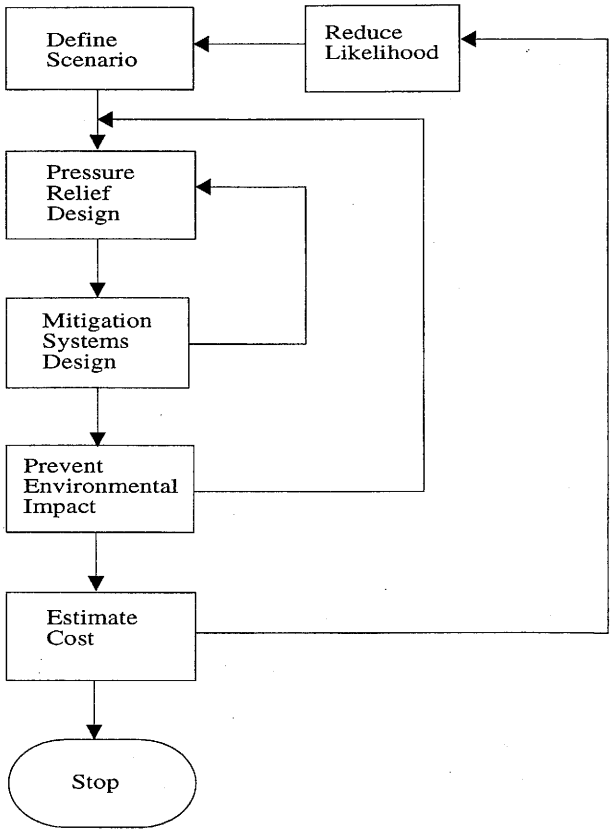

FIGURE 13. Typical emergency relief system design cycle.

5. Scaleup or Loading Factors, including credible heat influx from external fire events and physical characteristics of a full-scale containment vessel.
6. Vent Flow Characteristics, including multiphase/multicomponent system properties and effects of continuing chemical reaction.

The above data should be used in conjunction with the allowable design parameters (in terms of temperature, pressure and relief flow rate) of both the vessel and any requisite dump vessel/containment system to optimize the relief vent system design in terms of equipment, operator and environmental protection performance requirements.

In summary, a systematic approach to relief system design for reactive chemicals should be utilized to include evaluation of

1. chemical energy potential, i.e. thermochemistry,
2. chemical energy release rates, i.e. kinetics,
3. vessel response to internal pressure and thermal stress, and
4. reduction of hazard zones and environmental impact, i.e. collection and treatment of the discharge from the relief system.

In using this methodology we can encounter scenarios where one or more of the last two criteria specified above become either impossible or infeasible to engineer. In these situations, a process modification which eliminates or reduces the likelihood of the hazard scenario to an acceptable risk level is necessary. This process is shown graphically in Figure 13.

PRESSURE DEFINITIONS

Before discussing sizing methodologies we will define pressure terms frequently encountered in vent sizing:

- vent set pressure, P_{set}, i.e. the pressure at which the relief device actuates,
- maximum pressure reached in the vessel during relief actuation, P_{max}, i.e. after relief device actuation at P_{set} the pressure in the vessel continues to rise until it reaches P_{max}, and
- vessel design pressure or maximum allowable working pressure, P_{mawp}, i.e. the maximum permissible pressure at the top of the vessel at the normal operating temperature specified for that pressure (see ASME boiler and pressure vessel code [*33*]).

The ASME boiler and pressure vessel code [*33*] is a design standard which defines allowances for exceeding the vessel maximum allowable working pressure. Pressure vessels (excluding unfired steam boilers) should be protected by a pressure-relieving device that will prevent the pressure in the vessel from rising more than 10% (gage) or 3 psi, whichever is greater, above P_{mawp}. This allowance is increased to 16% (gage) or 4 psi, whichever is greater, when multiple devices are provided. Under external fire loading, a pressure-relieving device should be installed to protect against excessive pressure such that the vessel pressure is prevented from rising more than 21% above P_{mawp}.

For vessels having no permanent supply connections and used for storing nonrefrigerated liquefied compressed gases at ambient temperature, the pressure relief devices should be capable of preventing the pressure from rising in excess of 20% of P_{mawp}. The relief device set pressure should not exceed P_{mawp}. The vessel should have enough ullage to prevent a liquid full condition and P_{mawp} should be greater than the vapor pressure of the stored material at the maximum anticipated temperature (normally <320 K) that the gas will reach under ambient conditions.

Reaction heat should be treated as a process upset which requires that P_{max} should be less or equal to 1.1 P_{mawp}

$$P_{max} \leq [1.10 P_{mawp,gage}] + P_s \tag{15}$$

where P_s is the ambient pressure. The set pressure should be selected as low as practically possible.

VESSELS CONTAINING NONREACTIVE LIQUIDS

Vent sizing recommended by NFPA 30 [*24*] for vessels containing a volatile liquid and exposed to external fire is calculated based on the liquid evaporation rate and all vapor flow at the maximum allowable internal pressure

$$A_h = \delta \frac{qA_w}{G_v} \frac{M_w}{\lambda} \tag{16}$$

where M_w is the molecular weight of the flowing vapor, λ is the latent heat of vaporization of the liquid, δ is an environmental factor which accounts for effects of insulation and other mitigating measures on the fire heat flux, q is the fire heat flux, A_w is the vessel wetted area, A_h is the required vent area, and G_v is the vapor mass flux. Assuming ideal gas behavior and an adiabatic process with negligible wall friction effects, application of the mechanical energy balance yields an expression for an instantaneous vapor mass flux under nonchoked flow conditions:

$$G_v = C_d \sqrt{2P_{max}\rho_{max}\left(\frac{\gamma}{\gamma-1}\right)\left[\left(\frac{P_s}{P_{max}}\right)^{2/\gamma} - \left(\frac{P_s}{P_{max}}\right)^{\gamma+1/\gamma}\right]} \tag{17}$$

Under choked flow conditions, the vapor mass flux is calculated from:

$$G_v = C_d \sqrt{\gamma P_{max}\rho_{max}\left(\frac{2}{\gamma+1}\right)^{\gamma+1/\gamma-1}} \tag{18}$$

Choked flow (maximum flow rate) occurs at a critical pressure ratio of:

$$\left(\frac{P_s}{P_{max}}\right)_c = \left(\frac{2}{\gamma+1}\right)^{\gamma/\gamma-1} \tag{19}$$

Here P_{max} is the maximum pressure allowed during relief activation and ρ_{max} is the vapor density evaluated at the liquid saturation temperature corresponding to P_{max}. For vessels containing unstable/reactive liquids, NFPA 30 indicates that the effects of heat or gas resulting from polymerization, decomposition, condensation or self-reactivity must also be taken into account.

VESSELS CONTAINING REACTIVE LIQUIDS

Let us consider a vessel containing a liquid mixture undergoing a chemical reaction such as decomposition, reaction with other species of impurities, etc. Depending on their behavior, reactions of liquids can be divided into three categories.

Certain types of liquid reactions use available reaction energy to generate gaseous noncondensable reaction products such as hydrogen, nitrogen, etc. These reactions are referred to as "gassy" reactions. The total pressure reached in the vessel is equal to the gas pressure, i.e. pressure rises in the vessel due to mass addition in the vapor space.

Other types of liquid reactions use their reaction energy to supply boiling energy for the liquid before the formation of gaseous products, i.e. the heat of reaction is removed by the internal energy of vaporization. The reaction is therefore referred to as "tempered" by the heat of vaporization of the liquid. The total pressure in the vessel at any time is equal to the vapor pressure of the liquid.

Hybrid reaction systems possess both "tempered" and "gassy" features. Noncondensable gaseous products are formed prior to boiling, but the reaction is "tempered" by vapor depletion. The total pressure in the vessel is the sum of the liquid vapor pressure and the gas partial pressure.

For "gassy" systems, the rate of pressure rise is most important in finding the venting requirement. For "tempered" systems, the rate of temperature rise at the liquid saturation temperature corresponding to the vent set pressure is most important in determining the relief requirement. For "hybrid" systems, both the temperature and pressure rise rates at the tempering conditions are required to determine the relief requirement.

The rates of pressure and temperature rise depend on reaction rates. Computer simulation can be used to estimate vent sizes for systems where reaction rate data is available.

For complex reactions where kinetic data does not exist, necessary data for vent sizing can be obtained from bench-scale calorimetry. Commercial calorimeters such as the ARC[1] (Accelerating Rate Calorimeter), VSP[2] (Vent Sizing Package) [*34*, *35*]), RSST[3] (Reactive Systems Screening Tool) [*36*], etc. The ARC and VSP employ closed test cells while RSST uses an open glass bomb.

[1] ARC is a registered trademark of Columbia Scientific Industries.
[2] Manufactured by Fike Corporation
[3] Manufactured by Fauske & Associates, Inc.

Because small test cells (10 to 100 ml) are typically used in laboratory devices, thermal inertia corrections are necessary to scaleup measured data. The thermal inertia of a reactor vessel is often characterized using the following relation:

$$\Phi = 1 + \frac{M_{\text{vessel}} C_{v_{\text{vessel}}}}{M_l C_{v,l}} \tag{20}$$

Another factor which requires quantification is the effect of external fire or loss of cooling on reaction rates and vent sizing. This requires special device modification, or computer simulation with good kinetic data.

DETAILED KINETIC MODELING

Consider a vessel containing a reacting two-phase multicomponent mixture of total volume V, temperature T, and pressure P. Both the vapor and liquid phases are assumed to be in thermal, mechanical, and diffusional equilibrium. Neglecting liquid potential energy effects, the unsteady behavior of the system can be completely described based on first principles by writing the equations describing the internal energy change, the constant volume constraint, conservation of mass, and vapor-liquid equilibrium relations.

The overall internal energy change of the system is:

$$\left[N_{\text{metal}} C_{v_{\text{metal}}} + \sum_i^C (N_i + n_i) C_{v_i} + N_T \frac{\partial \Delta \underline{U}_v}{\partial T} + n_T \frac{\partial \Delta \underline{U}_l}{\partial T}\right] \frac{dT}{dt}$$
$$+ \left[N_T \frac{\partial \Delta \underline{U}_v}{\partial P} + n_T \frac{\partial \Delta \underline{U}_l}{\partial P}\right] \frac{dP}{dt}$$
$$+ \sum_i^C \left(\underline{U}_{i,\text{ref}} + \int_{T_{\text{ref}}}^{t} C_{v_i} dT + \Delta \underline{U}_v + N_T \frac{\partial \Delta \underline{U}_v}{\partial N_i}\right) \frac{dN_i}{dt}$$
$$+ \sum_i^C \left(\underline{U}_{i,\text{ref}} + \int_{T_{\text{ref}}}^{T} C_{v_l} dT + \Delta \underline{U}_l + n_T \frac{\partial \Delta \underline{U}_l}{\partial n_i}\right) \frac{dn_i}{dt}$$
$$= \dot{Q} - \dot{H}_{l,\text{out}} - \dot{E}_{l,\text{out}} - \dot{H}_{v,\text{out}} - \dot{E}_{v,\text{out}} \tag{21}$$

Here $\dot{Q}$ represents heat gained/lost by the vessel from/to the surroundings including fire loading and convective/conductive heat transfer and $\underline{U}_{i,\text{ref}}$ is the internal energy of formation of species i. The heat effects of any internal vessel components can be accounted for by adding the appropriate NC_v term to equation (21). It is interesting to note that the heat of reaction for any given reaction is implicitly added to removed from the system when the individual number of moles are changed.

The constant volume constraint is expressed as follows:

$$(V_v \beta_v + V_l \beta_l) \frac{dT}{dt} - (V_v \kappa_v + V_k \kappa_l) \frac{dP}{dt}$$
$$+ \sum_i \overline{V}_{v_i} \frac{dN_i}{dt} + \sum_i \overline{V}_{l_i} \frac{dn_i}{dt} = 0 \tag{22}$$

The conservation of mass equations are

$$\frac{dn_i}{dt} + \frac{dN_i}{dt} = -\dot{n}_{i,\text{out}} - \dot{N}_{i,\text{out}} + \dot{R}_i \text{ (for } i = 1, \cdots, C) \tag{23}$$

where $\dot{R}_i$ is the overall production rate of species i for all reactions involving the ith species.

The equilibrium relations between the vapor and the liquid phases are written as functions of the liquid and vapor fugacity coefficients:

$$\frac{N_i}{N_T} - \frac{n_i}{n_T} \frac{\hat{\phi}_{l,i}}{\hat{\phi}_{v,i}} = 0 \text{ (for } i = 1, \cdots, C) \tag{24}$$

For ideal systems, equation (24) can be rewritten as a function of the species saturation pressures:

$$\frac{N_i}{N_T} - \frac{n_i}{n_T} \frac{P_{\text{sat},i}}{P} = 0 \text{ (for } i = 1, \cdots, C) \tag{25}$$

Tempered, gassy and hybrid system behaviors are all described by equations (24) and (25), which determine the distribution of reaction products between the liquid and vapor phase.

Equations (21), (22), (23), and (24) yield $2C+2$ differential algebraic equations. These equations are solved using the semi-implicit Runge-Kutta algorithm of Michelsen [37]. This algorithm is applicable to the solution of simultaneous differential and nonlinear algebraic equations to include stiff systems.

The individual molar flow rates, $\dot{n}_i$ and $\dot{N}_i$, are determined at each time increment by maximizing mass flow at the nozzle and assuming quasi-steady and isentropic behavior with a specified void fraction/slip model.

The overall production rates of species i depend on many factors such as pressure, temperature, composition, solvent or other third body concentration, external heating, etc. Characterizing the overall production rates using detailed mechanistic kinetics is extremely difficult. What is done instead is to use global mechanisms to describe the overall production rates of any given species.

Global mechanisms are stoichiometric relations for which approximate kinetic expressions can be developed. A small number of steps are used to represent the behavior of a large number of reactions. These global mechanisms tend to involve only the major stable species. Minor species make little contribution to the energetics of the reaction system, but can influence the formation of pollutants.

Consider J global reversible (or irreversible) reactions involving C chemical species. We represent this reaction system in general form as

$$\sum_{i=1}^{C} \nu'_{ij} \chi_i \rightleftharpoons \sum_{i=1}^{C} \nu''_{ij} \chi_i \quad \text{for} \quad j = 1, \cdots, J \tag{26}$$

where ν is the stoichiometric coefficient and χ represents a chemical species. The superscript $'$ indicates a reactant, and $''$ indicates a product.

The overall production rate of the ith species is defined as

$$\dot{R}_i = \sum_{j=1}^{J} \nu_{ij} q_j \text{ for } i = 1, \cdots, C \tag{27}$$

where

$$\nu_{ij} = \nu''_{ij} - \nu'_{ij} \tag{28}$$

and q_j is the rate of progress for the jth reaction which is defined as

$$q_j = k_{f_j} \Pi_{i=1}^{C} [X_i]^{O'_{ij}} - k_{r_j} \Pi_{i=1}^{C} [X_i]^{O''_{ij}} \tag{29}$$

where $[X_i]$ is the molar concentration of the ith species and k_{f_j} and k_{r_j} are the forward and reverse rate constants of the jth reaction. O'_{ij} and O''_{ij} are the forward and reverse reaction orders and do not necessarily have to equal ν'_{ij} and ν''_{ij}. The forward rate expressions are assumed to obey an Arrhenius temperature dependence:

$$k_{f_j} = A_j \exp\left[\frac{-E_j}{R_g T}\right] \tag{30}$$

Typically the reverse constant is calculated using an equilibrium relationship

$$\frac{k_{f_j}}{k_{r_j}} = K_{c_j} \tag{31}$$

where K_{c_j} is an equilibrium constant in concentration units. All chemical reactions are reversible to some extent. A completely irreversible reaction implies an infinite change in Gibbs free energy. Reactions involving large free energy changes are practically irreversible. For reversible chemical reactions, the reverse rate constant of reaction j, k_{r_j}, can be estimated from thermodynamics. If the value of the forward reaction rate is known, then

$$k_{r_j} = \frac{k_{f_j}}{K_{c_j}} \tag{32}$$

where

$$K_{c_j} = K_{p_j}\left[\frac{1}{ZR_gT}\right]^{\Sigma_{i=1}^{C}\nu_{ij}}\left[\frac{1}{K_{\Phi_j}}\right] \tag{33}$$

K_{Φ_j} represents a nonideal contribution to the equilibrium constant for reaction j

$$K_{\Phi_j} = \Pi\hat{\Phi}_i^{\nu_{ij}} \tag{34}$$

where $\hat{\Phi}_i$ is the fugacity coefficient of species i.

The equilibrium constant K_{p_j} is a function of temperature only:

$$\ln K_{p_j} = -\frac{\Sigma_{i=1}^{C}\nu_{ij}\underline{G}_j}{R_gT} \tag{35}$$

K_{p_j} can also be expressed as a function of ideal gas entropies and enthalpies:

$$\ln K_{p_j} = \sum_{i=1}^{C}\nu_{ij}\frac{\underline{S}_{i,f,T_0} + \int_{T_0}^{T}\frac{C_{p_i}}{T}dT}{R_g} - \sum_{i=1}^{C}\nu_{ij}\frac{\underline{H}_{i,f,T_0} + \int_{T_0}^{T}C_{p_i}dT}{R_gT} \tag{36}$$

Analytic expressions for activation energy and reaction order can be derived for nonreversible, nonautocatalytic reactions involving one species. A reaction order of o and involving a single reactant is represented as follows:

$$\frac{d[X]}{dt} = -\nu k_f[X]^O \tag{37}$$

Assuming a constant heat of reaction, the molar concentration can be represented by temperature using the folllowing relation:

$$\frac{[X]}{[X_0]} = \eta = \frac{T_f - T}{T_f - T_0} \tag{38}$$

where T_f is the final temperature measured at a heating rate of 0.02 C/min and T_0 is the initial temperature measured at a heating rate of 0.02 C/min.

Differentiation of equation (38) and substitution into equation (37) yields the following relation for temperature rise rate:

$$\frac{dT}{dt} = \nu k_f[X_0]^{O-1}\eta^O[T_f - T_0] \tag{39}$$

where η is defined earlier.

A heat rate can be obtained at any temperature by substituting an expression for k_f in the above equation.

$$\left[\frac{dT}{dt}\right] = \left[\frac{dT}{dt}\right]_0 \eta^O \exp\left[\frac{E}{R}\left(\frac{1}{T_0} - \frac{1}{T}\right)\right] \tag{40}$$

The reaction order can be obtained by setting the second derivative of equation (39) to 0 and substituting the temperature at the peak heating rate T_{max} for T:

$$O = \frac{E}{R}\frac{T_f - T_{max}}{T_{max}^2} \tag{41}$$

where O is different from 0.

A kinetic rate constant is obtained by rearranging equation (38) to give:

$$\nu k_f[X_0]^{O-1} = \frac{\frac{dT}{dt}}{\eta^O(T_f - T_0)} \tag{42}$$

A plot of the logarithm of the left hand side of equation (42) vs. $1/T$ should yield a straight line with a slope of E/R and an intersect equal to the log of the preexponential factor.

For systems with complicated reaction mechanisms, kinetic data can be obtained by simulating the experiment using a comprehensive model for a closed test cell such as provided by the ARC. Once the number of reactions, stoichiometry and reaction products are specified, an iterative nonlinear regression analysis is used to determine the activation energies, reaction orders and preexponential factors for all reactions involved. These parameters are adjusted until the sums of squares of the difference between predicted and actual pressure and temperature histories are minimized.

ESTABLISHING REACTION STOICHIOMETRY

The use of adiabatic/constant volume kinetic data for emergency relief systems design requires that the reaction stoichiometry and the chemical identity of the products be known. Both the stoichiometry and the chemical identity of the products are implicit in the measured pressure/temperature data at constant volume.

The pressure/temperature relation is a function of thermal inertia, liquid fill level (vessel void fraction), composition and chemical identity (vapor-liquid equilibria, liquid/vapor density, heats of formation, etc). For a specified relief device set pressure, there is a unique corresponding system temperature. For reactive systems, this temperature corresponds to a reaction rate. Small errors in estimating the temperature at the relief device set pressure for reactive systems can lead to inadequate sizing and potential catastrophic vessel failure. For emergency relief systems design, the pressure/volume/temperature (PVT) relation of a reactive or nonreactive system is a fundamental and unique relation that must be accurately represented during direct scaleup or computerized simulation. Variables which can significantly alter the PVT behavior of a system should be quantified.

Estimation of fluid flow rates and their associated energy depletion rates is a strong function of chemical identity. A

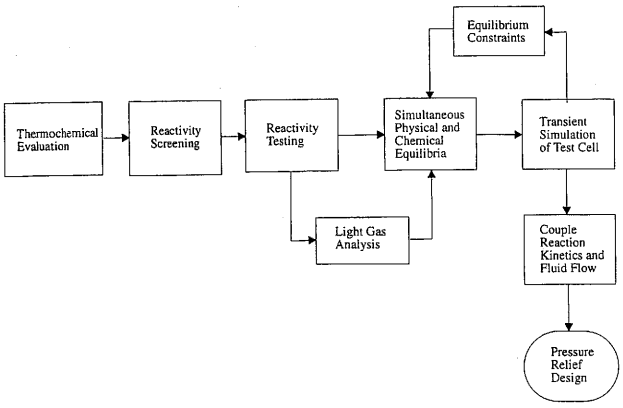

FIGURE 14. An integrated approach to emergency relief design for reactive systems.

serious error is made by establishing a reaction model which will only fit the observed constant volume pressure/temperature relation and temperature/pressure time histories. This is done by assuming, for example, the reaction products are made of a heavy and a light and by independently specifying a heat of reaction. However, this alone does not guarantee a unique solution, i.e. the chemical identities of the products are not unique. When applying this type of a simple model for emergency systems relief design, estimated flow rates are often in error.

A unique solution can be guaranteed by requiring that the reaction stoichiometries and chemical identities of the products are thermochemically favorable. This can easily be done by performing a multiphase simultaneous physical and chemical equilibrium calculation at constant volume for any proposed stoichiometry and product list. This is typically done be direct minimization of the Gibbs free energy. For systems involving large numbers of degrees of freedom (reactions and species), obtaining the exact stoichiometry and species identity can be a formidable task. We can however, simplify and constrain the equilibrium calculation in order to narrow the search space as follows:

1. Volume, pressure and adiabatic temperature rise must match observed experimental values.
2. The final cooldown pressure/temperature conditions at constant volume yield a certain ratio of noncondensables/volatiles which must be reflected by the identity of any proposed reaction products.
3. Light gas analysis can be obtained and used to specify the identity of all or some of the reaction products.

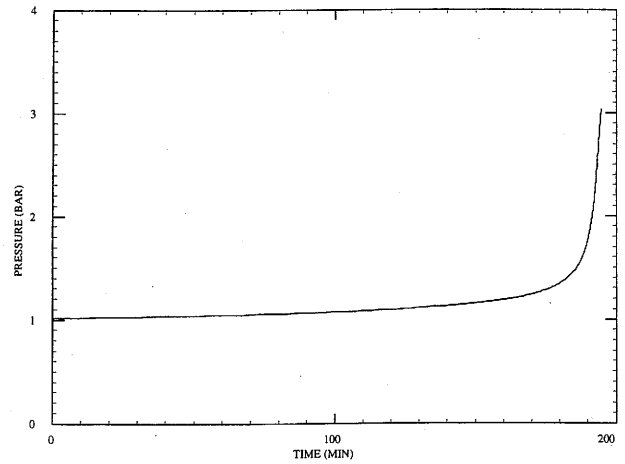

FIGURE 15. Constant volume pressure-time history for the acetic anhydride/methanol esterification reaction.

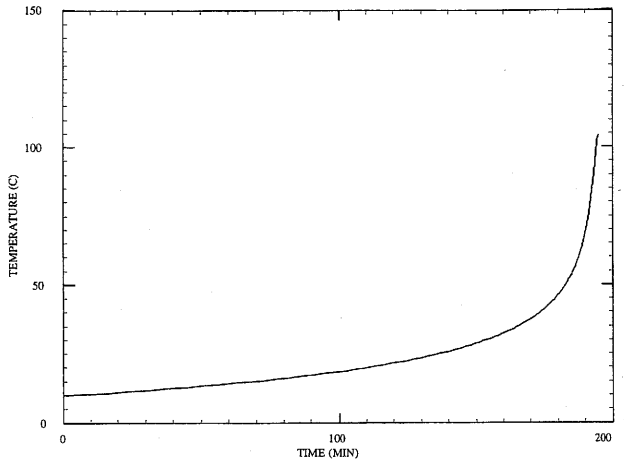

FIGURE 16. Constant volume temperature-time history for the acetic anhydride/methanol esterification reaction.

These types of constraints can be imposed as additional atom matrix constraints for the Gibbs free energy minimization and will serve to reduce the search space for rate-limiting reaction steps. Clearly, this type of analysis can be useful in obtaining global reaction rate models from constant volume adiabatic small-scale tests. The following assumptions are implicit in this methodology:

1. Slow reactions are the passive constraints that will retard the relaxation of the system for reaching complete equilibrium,
2. Fast reactions will equilibrate the system subject to the constraints imposed by the slow reactions and
3. The system will proceed to complete equilibrium through a sequence of constrained equilibrium states at a rate controlled by the slow reaction steps.

We have streamlined this analysis and linked the constrained minimization code with an extensive properties database. The stoichiometry/chemical identity program executes the following steps:

1. Select all species with similar atomic constituents from the database. For example if H_2O was a reactant, the program would select H_2, O_2, O_3, OH, H, etc.
2. Rank by increasing Gibbs free energy at the system temperature and pressure.

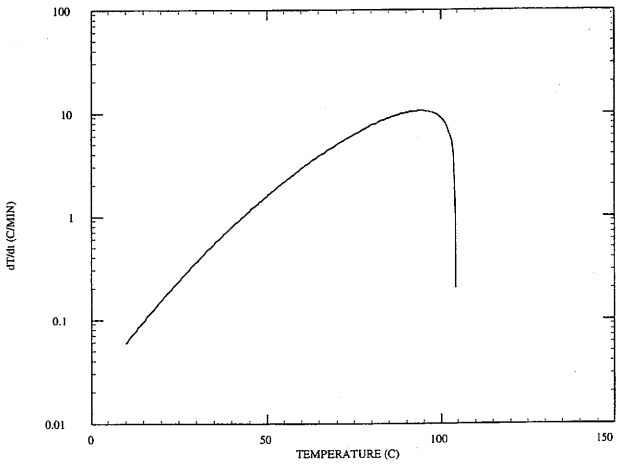

FIGURE 17. Constant volume temperature rise rate history for the acetic anhydride/methanol esterification reaction.

Table 3 Constrained Gibbs Free Energy Minimization Data for Methanol/Acetic Acid Esterification

	Case 1	Case 2	Case 3
Atom and Constraints Matrix rank	5	6	7
Maximum number of independent reactions	98	97	96
Scaled Gibbs free energy	−9493	−7688	−7469
Initial temperature (K)	283	283	283
Final temperature (K)	377	377	377
Initial pressure (Pa)	101325	101325	101325
Final pressure (Pa)	299000	299000	299000
Initial number of moles (kmol)	335.798	335.798	335.798
Final number of moles (kmol)	422.917	343.440	335.798
Change in number of moles (kmol)	87.119	7.642	0
Initial volume (m^3)	10.6	10.6	10.6
Final volume (m^3)	1561	37.2	10.3
Volume change (m^3)	1550.4	26.4	−0.3
Initial enthalpy (MJ)	82800	82800	83800
Final enthalpy (MJ)	82600	81972	82860
Enthalpy change (MJ)	−200	−828	−60

3. Select top 100 species.
4. Impose constraints using observed data.
5. Perform simultaneous physical/chemical equilibria.

Once the global stoichiometry is identified, the detailed methods described earlier for simulating reacting systems in vessels are used as follows to determine the reaction rates:

1. Guess reaction(s) order, preexponential factor(s) and activation energies.
2. Simulate test cell including heat-up period (heat/wait).
3. Calculate the sum of squares for T/P, T/time, and P/time.
4. If minimum is not reached, go to step 1.

Scaleup is then achieved by using the same model for transient temperature, pressure, and flow estimates for plant vessels under fire exposure or process upsets. This scaleup takes into account the size, configuration and operating conditions of the plant equipment, the extent of mixing, natural cooling losses and forced cooling capacity, vessel insulation, wall conductivity, etc. This integrated approach to ERS design for reactive systems is illustrated in Figure 14. We will illustrate the use of closed volume data to find reaction stoichiometry and kinetic information for the esterification reaction of methanol and acetic anhydride. Figures 15, 16, and 17 illustrate the pressure-time, temperature-time, and temperature rise rate data observed experimentally using the ARC. The sample size used was five grams and consisted of 69.7 mole % acetic anhydride and 29.9 mole % methanol (acetic anhydride is in excess). The initial temperature and pressure were at 283 K and 101325 Pa with a nitrogen pad. The amount of nitrogen present in the bomb at the start is estimated at 0.415 mole %. The final cooldown pressure was measured to be slightly above atmospheric pressure at 298 K. Chemical analysis was not performed on the reaction products to determine their identity. The peak temperature was measured to be 377 K and the corresponding peak pressure was measured to be 299000 Pa. The bomb volume was 10 mL and has an equivalent thermal heat capacity of 15.3 g of iron.

We followed the constrained equilibrium method outlined in this paper and selected (for illustration purposes) 50 chemical species as potential reaction products. We then conducted three P/T simulations to match the peak temperature and pressure conditions measured in the experiment. These estimates are summarized in Table 3 with solid-vapor-liquid molar distributions reported in Tables 4 and 5. Iron was used to simulate the bomb thermal inertia and all quantities are scaled up to a kilomole and cubic meter basis to avoid numerical roundoff errors.

Case 1 represents an unconstrained simulation. All the reactants are consumed and no liquid phase is predicted for the reaction products. From Table 3 we note that to match the experimental peak temperature and pressure values, a volume change of 1550.4 m^3 and an exothermic enthalpy change of −200 MJ are required. This clearly does not represent the measured constant volume data.

Case 2 is a repeat of case 1 with one additional constraint. This constraint specifies that all reaction products are volatiles, i.e. (with the exception of nitrogen) noncondensables are not present as products. This is in agreement with the reported final cooldown pressure. We note from Table 3 that the minimum Gibbs free energy calculated is larger than that of case 1 and that the maximum number of independent reactions has decreased by one degree of freedom. The calculated change in volume and enthalpy at 377 K and 299000 Pa still do not match the experimental data.

Case 3 is a repeat of case 2 with one additional constraint. This second constraint specifies (based on chemical grounds) that the total number of moles has to remain constant, i.e. the number of moles of reactants is equal to the number of moles of products. Table 3 shows a good agreement between predicted and reported constant volume data. Tables 4 and 5 show that equimolar amounts of methyl acetate and acetic acid are formed and that all the methanol is converted. Small amounts of ethylene glycol, n-propionaldehyde and ethyl formate are also formed. The negative overall volume change is due to the absence of binary interaction parameters for the equation of state, i.e. zero values are used. BIPS values need to be estimated for systems which exhibit strong solution nonidealities.

The esterification of methanol/acetic anhydride is a well studied reaction which is known to yield methyl acetate and acetic acid. Using the reaction stoichiometry predicted by the equilibrium code and simulation of the test data yield an excellent agreement between the entire measured and predicted pressure-temperature, pressure-time, temperature-time and temperature rise rate.

Chemical analysis of the liquid phase and/or vapor phase can provide useful additional constraints. The amounts of the identified species do not need to be very accurate as long as the molar ratios (which serve as constraints) are. This method can be applied to more complicated reaction schemes. A detailed and robust simultaneous chemical and physical equilibrium is required, however. Theoretically, we may need as many constraints as the number of the degrees of freedom in order to completely specify the system. We have, to date, applied this technique to more than thirty complex systems and used no more than a total of six constraints.

Table 4 Constrained Gibbs Free Energy Minimization Data for Methanol/Acetic Anhydride Esterification. Solid/Vapor Molar Distribution (kmol)

Component/Phase	Initial	Case 1	Case 2	Case 3
Iron (S)	273.950	273.950	273.95	273.95
Acetic Anhydride (V)			0.05035	0.01970
Methanol (V)				
Nitrogen (V)	0.25664	0.25664	0.24848	0.20925
Carbon Dioxide (V)		71.6930	0.00381	
Acetic Acid (V)			0.36491	0.02940
Formic Acid (V)			0.00121	
Methyl Acetate (V)				0.18591
Ethylene Glycol (V)				
Methyl Formate (V)			0.00022	
Ethyl Formate (V)				0.00046
Methyl Acrylate (V)			0.04029	
Water (V)			0.00068	
beta-Propiolactone (V)				
Vinyl Acetate (V)				
Vinyl Formate (V)				
Carbon Monoxide (V)		4.41002		
Glyoxal (V)				
Diketene (V)			0.00040	
Acetaldehyde (V)			0.00092	
Formaldehyde (V)				
n-Propionaldehyde (V)			0.00432	0.00103
Hydrogen Peroxide (V)				
Dimethyl Ether (V)				
Ketene (V)			0.00093	
Allyl Alcohol (V)				
Acrolein (V)			0.03141	
Methane (V)		51.5319		
Methacrolein (V)		0.00007	0.27799	
trans-Crotonaldehyde (V)			0.01838	
Methyl Vinyl Ether (V)				
2.5-Dihydrofuran (V)			0.00027	
Ethane (V)		7.83576		
1,2-Propylene Oxide (V)				
Hydrogen (V)				
Oxygen (V)				
Ethylene Oxide (V)				
1,3-Propylene Oxide (V)				
Divinyl Ether (V)				
Ethylene (V)		0.00549		
Propargyl Alcohol (V)				
Propylene (V)		5.35822	1.65796	
Cyclopropane (V)				
1,3-Butadiene (V)		7.87622	0.30041	
Methylacetylene (V)				
Dimethylacetylene (V)		0.00020	0.00002	
Acetylene (V)				
Propadiene (V)				
1,2-Butadiene (V)				
Ethylacetylene (V)			0.00089	
Vinylacetylene (V)				

Table 5 Constrained Gibbs Free Energy Minimization Data for Methanol/Acetic Anhydride Esterification. Liquid Molar Distribution (kmol)

Component/Phase	Initial	Case 1	Case 2	Case 3
Acetic Anhydride (L)	43.10200		20.62222	24.67269
Methanol (L)	18.49016			
Nitrogen (L)			0.00815	0.04739
Carbon Dioxide (L)			0.00312	
Acetic Acid (L)			40.9804	18.46073
Formic Acid (L)			0.00277	
Methyl Acetate (L)			0.00196	18.02022
Ethylene Glycol (L)				0.08052
Methyl Formate (L)			0.00037	
Ethyl Formate (L)				0.04255
Methyl Acrylate (L)			0.14814	
Water (L)			0.00081	
beta-Propiolactone (L)			0.00139	
Vinyl Acetate (L)				
Vinyl Formate (L)				
Carbon Monoxide (L)				
Glyoxal (L)				
Diketene (L)				
Acetaldehyde (L)			0.00126	
Formaldehyde (L)			0.00038	
n-Propionaldehyde (L)			0.02116	0.07831
Hydrogen Peroxide (L)				
Dimethyl Ether (L)				
Ketene (L)				
Allyl Alcohol (L)			0.00031	
2-Butyne-1,4-Diol (L)				
Acrolein (L)			0.00035	
Methane (L)				
Methacrolein (L)			0.68495	
trans-Crotonaldehyde (L)			1.61204	
Methyl Vinyl Ether (L)				
2.5-Dihydrofuran (L)			0.02429	
Ethane (L)				
1,2-Propylene Oxide (L)				
Hydrogen (L)				
Oxygen (L)				
Ethylene Oxide (L)				
1,3-Propylene Oxide (L)				
Divinyl Ether (L)				
Ethylene (L)				
Propargyl Alcohol (L)				
Propylene (L)			1.58132	
Cyclopropane (L)			0.00038	
1,3-Butadiene (L)			0.78737	
Methylacetylene (L)				
Dimethylacetylene (L)			0.00184	
Acetylene (L)				
Propadiene (L)			0.00073	
1,2-Butadiene (L)			0.00118	
Ethylacetylene (L)			0.00015	
Vinylacetylene (L)				

VAPOR-LIQUID EQUILIBRIUM DATA

The Accelerating Rate Calorimeter (ARC) is an instrument that can provide adiabatic pressure and temperature time data required for establishing reaction stoichiometry and pressure relief design. This instrument which was developed by Townsend and Tou [*38*] and [*39*] is known to provide ample thermokinetic data that is applicable to the design and safety/performance evaluation of reactors and storage vessels. Such thermokinetic data includes:

- adiabatic rate of self-heating,
- adiabatic time of explosion,
- rate of pressure rise,
- maximum rate of reaction,
- kinetic data such as activation energy, reaction order and preexponential factor, and
- heat of reaction.

The ARC can also provide pressure-volume-temperature (PVT) data for pure components (vapor pressure) and mixtures (vapor-liquid equilibria). Measured PVT data can be used with the aid of an equation of state to estimate liquid density, liquid heat capacity, latent heat of vaporization, nonideal solution

Table 6 Equation of State Binary Interaction Parameters used to Describe the System Chloroacetyl Chloride, Water, Chloroacetic Acid, Hydrogen Chloride and Nitrogen

Component 1	Component 2	$k_{1,2}$	$\lambda_{1,2}$
Water	Hydrogen chloride	−0.8030	−1.0500
Water	CAC	−0.0513	−0.1950
Water	CAA	−0.1110	0.0417
Water	Nitrogen	0.0000	0.0000
Hydrogen chloride	CAC	0.0021	−0.0081
Hydrogen chloride	CAA	−0.0267	0.0023
Hydrogen chloride	Nitrogen	0.0000	0.0000
CAC	CAA	−0.0135	0.0054
CAC	Nitrogen	0.0000	0.0000

thermodynamics, and most importantly vapor-liquid equilibrium data which is crucial for pressure relief design, especially for reactive systems.

We illustrate the ability of the ARC to measure vapor-liquid equilibrium by providing data for a 50/50 mixture (by weight) of acetone-water. The system acetone-water was selected as an illustration because of its nonideal behavior and because of the availability of ample experimental VLE data measured by other methods. A total of 6.560 grams of acetone-water mixture is placed in a titanium bomb at 303 K and 1 bar under a nitrogen gas pad. The titanium bomb mass is 8.854 grams and its volume is 9.8 ml. Figure 18 compares the measured pressure/temperature data from the ARC for the system nitrogen-acetone-water to model predictions using binary interaction parameters (BIPS) determined by Melhem *et al.* [*40*] from VLE measurements by different investigators.

- acetone-water, $k_{ij} = -0.17643$, $\lambda_{ij} = 0.14203$,
- acetone-nitrogen, $k_{ij} = -0.16835$, $\lambda_{ij} = 0.002526$, and
- water-nitrogen, $k_{ij} = -0.98224$, $\lambda_{ij} = 0.011908$.

As show by Figure 18, the agreement is excellent over a wide temperature range. The values of k_{ij} and λ_{ij} can be obtained using least squares minimization:

1. Guess k_{ij} and λ_{ij}.
2. Simulate test cell.
3. Minimize the sum of squares between measured and predicted P/T histories.
4. If minimum is not reached, go to 1.

This procedure can be used to verify or estimate PVT/VLE behavior using data collected during the heat-wait-search period.

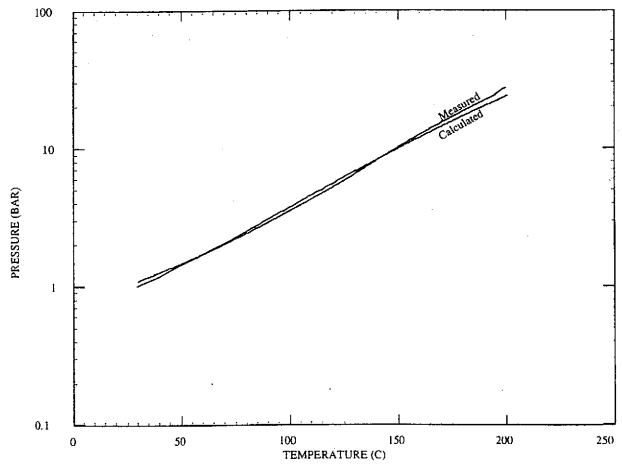

FIGURE 18. Acetone-water-nitrogen vapor-liquid equilibrium ARC data.

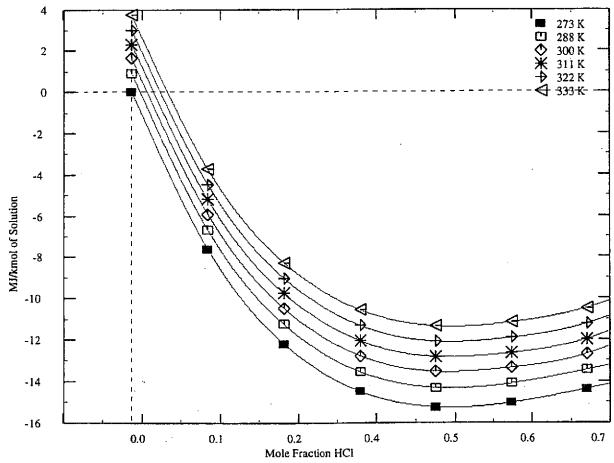

FIGURE 19. Enthalpy-concentration chart of hydrogen chloride-water solutions relative to pure hydrogen chloride gas and water liquid at 273 K and 1 atmosphere.

NONIDEAL SOLUTION BEHAVIOR

The constant volume mass and energy balance equations derived in the previous sections are general and implicitly represent fluid nonideal behavior caused by solution behavior, system pressure and temperature. The partial molar properties are calculated from an equation of state (EOS) with suitable binary interaction parameters (BIPs). BIPs are typically estimated from experimental VLE data or predicted using group contribution methods. Also implicit in the general formulation is the heat generation or removal caused by chemical reaction as the number of moles of reacting species changes.

We illustrate the use of the EOS approach adopted in the detailed formulation of mass and energy balances on hydrogen chloride and water solution behavior. Figure 19 illustrates an enthalpy-concentration diagram estimated using the EOS approach for hydrochloric acid solutions relative to pure hydrogen chloride (gas) and water (liquid) at 273.15 K and 1 atmosphere. The EOS binary interaction parameters for hydrogen chloride and water estimated from experimental VLE data are:

$$k_{1,2} = -0.803 = k_{2,1} \tag{43}$$

$$\lambda_{1,2} = 1.05 = -\lambda_{2,1} \tag{44}$$

The predicted data shown in Figure 19 is in excellent agreement with the experimental data on heat of solution for hydrogen chloride—water solution reported by Hougen and Watson in reference [*41*].

Figure 19 is useful for the estimation of final mixture temperature when mixing solutions of varying hydrogen chloride concentration. For example, if we were to mix 0.263 kmol of a 10% by weight (5.26 mol %) mixture of hydrogen chloride and water at 288 K with a mixture containing 30% by weight (17.6 mol %) hydrogen chloride and water, what would be the final mixture temperature?

The enthalpy of each of the two solution mixes is read from Figure 19. The 10% solution enthalpy is −3.5 MJ/kmol or −0.92 MJ, and the 30% solution enthalpy is −8.00 MJ/kmol or −3.024 MJ. The mixture enthalpy is calculated to be −3.944 MJ or −6.15 MJ/kmol. Upon mixing, the final mixture composition would be 12.53 mol % hydrogen chloride. Using a mole fraction of 12.53% and a molar enthalpy of −6.15 MJ/kmol, we can read from Figure 19 a temperature of 305.5 K or 89.9 F. Hougen and Watson [*41*] report a temperature of 90 F for the same problem.

We consider another example to illustrate how nonideal solution behavior can alter the pressure-temperature behavior of

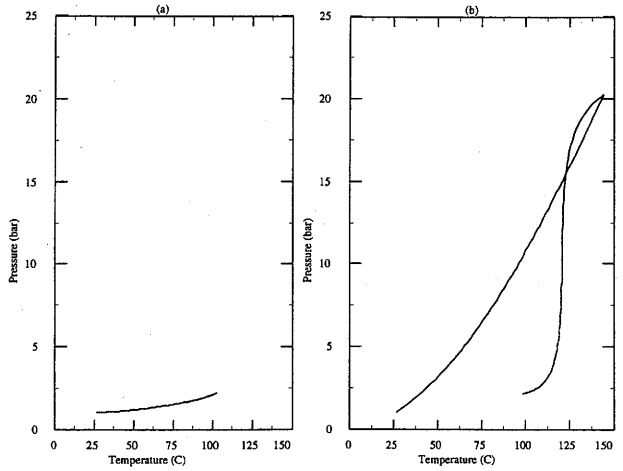

FIGURE 20. Nonideal solution behavior impact on closed vessel pressure-temperature behavior for chloroacetyl chloride/water system.

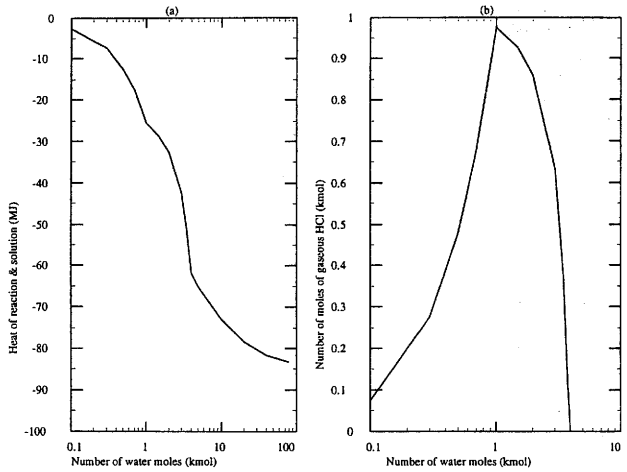

FIGURE 21. Nonideal solution thermodynamics for the system chloroacetyl chloride, water, chloroacetic acid and hydrogen chloride. Bases = 1 kmol of chloroacetyl chloride, 298 K, 1 bar, open volume.

systems where hydrogen chloride and water are generated by a chemical reaction. Two cases are considered:

(a) A vessel initially contains 1000 kg of water (55.5 kmol) at 300 K and 1 bar. The total vessel volume is 9.2 m^3. 622 kg (5.5 kmol) of liquid chloroacetyl chloride (CAC) is pumped into the liquid space at 0.00925 kmol/s. The CAC entering the vesssel is at 300 K and 1 bar and is immediately mixed with the water due to the action of an agitator. Mixing is sufficient to cause an immediate reaction between CAC and water to generate hydrogen chloride and chloroacetic acid (CAA):

$$C_2H_2Cl_2O + H_2O \rightarrow C_2H_3ClO_2 + HCl \qquad (45)$$

The vessel space contains nitrogen.

(b) The case is similar to case a. The vessel initially contains 622 kg of CAC and water is pumped into the vessel at the rate of 0.00925 kmol/s.

Figure 20 illustrates the behavior of pressure-temperature for both cases. For case (a), as CAC is pumped into the vessel, it mixes with water and immediately reacts to generate hydrogen chloride which goes into solution as the ratio of water to CAC is 10 to 1. A peak pressure of 2.2 bar is reached at 100 C. For case (b), water is pumped into the vessel, mixes with CAC and generates hydrogen chloride which has a limited solubility in chloroacetyl chloride and CAA. As a result, the pressure and temperature increase steadily. As the CAC is depleted and more water is added, the hydrogen chloride goes into solution. The final vessel conditions are the same as in case (a) with a peak pressure of 20.2 bar. Figure 21 shows a similar behavior for the same system at 1 bar. Figure 21-a illustrates the effect of water to CAC molar ratio on the combined net heat of solution and reaction. At a molar ratio of 1, the heat of reaction is -25 MJ/kmol. Figure 21-b indicates that all evolved hydrogen chloride is gaseous when the molar ratio of water to CAC is less or equal to 1, i.e. CAC is in excess of stoichiometric. As excess water is added, the hydrogen chloride goes into solution. At a molar ratio of water to CAC greater than or equal to 4, all evolved hydrogen chloride is retained in the liquid phase. The heat of solution effects are shown in Figure 21.

The pressure-temperature behavior is a key relation for pressure relief design. Nonideal solution behavior plays a key role in the interpretation of experimental data and scaleup. This is similar to concepts taught in general chemistry about adding acid to water!

VESSELS CONTAINING VAPORS

Consider a vessel containing a multicomponent vapor mixture, of total volume V, temperature T, and pressure P. The unsteady behavior of the system can be completely described based on first principles by writing the equations describing the internal energy change, the constant volume constraint, and conservation of mass. The overall internal energy change of the system is:

$$a\frac{dT}{dt} + b\frac{dP}{dt} = c \qquad (46)$$

where a, b, and c are constants defined as follows:

$$a = N_{\text{metal}}C_{v_{\text{metal}}} + \sum_i^C N_i C_{v_i} + N_T\frac{\partial \Delta \underline{U}_v}{\partial T}$$

$$b = N_T\frac{\partial \Delta \underline{U}_v}{\partial P}$$

$$c = \dot{Q} - \dot{H}_{v,\text{out}} - \dot{E}_{v,\text{out}} - \sum_i^C\left(\int_{T_{\text{ref}}}^{T} C_{v_i}dT + \Delta \underline{U}_v + N_T\frac{\partial \Delta U_v}{\partial N_i}\right)\frac{dN_i}{dt}$$

$\dot{Q}$ is external heat addition to/removal from the vessel. To reduce the internal pressure for vessels containing vapor exposed to fire, vapor must be removed at a sufficient rate to offset the change in density of the vessel vapor during pressure reduction.

The constant volume constraint is expressed as follows:

$$\beta_v\frac{dT}{dt} - \kappa_v\frac{dP}{dt} = -\frac{1}{V_v}\sum_i \overline{V}_{v_i}\frac{dN_i}{dt} \qquad (47)$$

The conservation of mass equations are:

$$\frac{dN_i}{dt} = -\dot{N}_{i,\text{out}} + \dot{R}_i \text{ (for } i = 1, \cdots, C) \qquad (48)$$

Equations (46), (47) and (48) yield $C+2$ ordinary differential equations. The individual molar flow rates $\dot{N}_{i,\text{out}}$, are determined at each time increment by maximizing mass flows at the nozzle, assuming quasi-steady and isentropic behavior.

REACTING FLOW IN PIPES/DUCTS

As in the case of a constant volume reacting system which was discussed earlier, we can write one-dimensional conservation equations and equilibrium relations for the combined liquid and vapor phases flowing in a pipe or duct with a constant cross-sectional area and at steady state:

Mass:

$$\dot{M}_T = \sum_j^C \dot{N}_j M_{w_j} = \rho_v u_v \alpha A \tag{49}$$

$$\dot{m}_T = \sum_j^C \dot{n}_j M_{w_j} = \rho_l u_l (1-\alpha) A \tag{50}$$

$$\frac{d\dot{n}_i}{dz} + \frac{d\dot{N}_i}{dz} = A\dot{R}_i \text{ (for } i = 1, \cdots, C) \tag{51}$$

Momentum:

$$\frac{dP}{dz} + \frac{1}{A}\frac{d}{dz}[\dot{M}_T u_v + \dot{m}_T u_l = -\left[\frac{dP}{dz}\right]_F - g\rho_m \sin\theta \tag{52}$$

Energy:

$$\frac{d}{dz}\left[\dot{H}_v + \dot{H}_l + \frac{\dot{m}_T u_l^2}{2} + \frac{\dot{M}_T u_v^2}{2}\right] + (\dot{m}_T + \dot{M}_T) g \sin\theta = \frac{d\dot{Q}}{dz} - \frac{d\dot{W}}{dz} \tag{53}$$

Equilibrium:

$$\left[\frac{\Phi_i^v \dot{N}_i}{\dot{N}_T}\frac{\partial \ln \Phi_i^v}{\partial T} - \frac{\Phi_i^l \dot{n}_i}{\dot{n}_i}\frac{\partial \ln \Phi_i^l}{\partial T}\right]\frac{dT}{dz} + \left[\frac{\Phi_i^v \dot{N}_i}{\dot{N}_T}\frac{\partial \ln \Phi_i^v}{\partial P} - \frac{\Phi_i^l \dot{n}_i}{\dot{n}_T}\frac{\partial \ln \Phi_i^l}{\partial P}\right]\frac{dP}{dz} + \sum_j^C\left[-\frac{\Phi_i^v \dot{N}_i}{\dot{N}_T^2} + \frac{\Phi_i^v \dot{N}_i}{\dot{N}_T}\frac{\partial \ln \Phi_i^v}{\partial \dot{N}_j}\right]\frac{d\dot{N}_j}{dz} + \frac{\Phi_i^v}{\dot{N}_T}\frac{d\dot{N}_i}{dz} + \sum_j^C\left[\frac{\Phi_i^l \dot{n}_i}{\dot{n}_T^2} - \frac{\Phi_i^l \dot{n}_i}{\dot{n}_T}\frac{\partial \ln \Phi_i^l}{\partial \dot{n}_j}\right]\frac{d\dot{n}_j}{dz} - \frac{\Phi_i^l}{\dot{n}_T}\frac{d\dot{n}_i}{dz} = 0 \quad (i = 1, \cdots, C) \tag{54}$$

where

$$\rho_m = \alpha\rho_v + (1-\alpha)\rho_l \tag{55}$$

$$\dot{n}_T = \sum_j^C \dot{n}_j \tag{56}$$

$$\dot{N}_T = \sum_j^C \dot{N}_j \tag{57}$$

$$\frac{d\dot{H}_v}{dz} = \underbrace{\left[\sum_j^C \dot{N}_j Cp_j + \dot{N}_T\frac{\partial \Delta\underline{H}_v}{\partial T}\right]}_{E_0}\frac{dT}{z} + \underbrace{\left[\dot{N}_T\frac{\partial \Delta\underline{H}_v}{\partial P}\right]}_{E_1}\frac{dP}{dz} + \underbrace{\sum_j^C\left(\underline{H}_{j,\text{ref}} + \int_{T_{\text{ref}}}^T Cp_j dT + \Delta\underline{H}_v + \dot{N}_T\frac{\partial \Delta\underline{H}_v}{\partial \dot{N}_j}\right)\frac{d\dot{N}_j}{dz}}_{E_n} \tag{58}$$

$$\frac{d\dot{H}_l}{dz} = \left[\sum_j^C \dot{n}_j Cp_j + \dot{n}_T\frac{\partial \Delta\underline{H}_l}{\partial T}\right]\frac{dT}{dz} + \left[\dot{n}_T\frac{\partial \Delta\underline{H}_l}{\partial P}\right]\frac{dP}{dz} + \sum_j^C\left(\underline{H}_{j,\text{ref}} + \int_{T_{\text{ref}}}^T Cp_j dT + \Delta\underline{H}_l + \dot{n}_T\frac{\partial \Delta\underline{H}_l}{\partial \dot{n}_j}\right)\frac{d\dot{n}_j}{dz} \tag{59}$$

$$\frac{d\rho_v}{dz} = \underbrace{\rho_v\kappa_v}_{R_1}\frac{dP}{dz} - \underbrace{\rho_v\beta_v}_{R_0}\frac{dT}{dz} + \underbrace{\frac{\rho_v}{\dot{M}_T}\sum_j^C [M_{w_j} - \rho_v \overline{V}_{vj}]\frac{d\dot{N}_j}{dz}}_{R_n} \tag{60}$$

$$\frac{d\rho_l}{dz} = \rho_l\kappa_l\frac{dP}{dz} - \rho_l\beta_l\frac{dT}{dz} + \frac{\rho_l}{\dot{m}_T}\sum_j^C [M_{w_j} - \rho_l \overline{V}_{lj}]\frac{d\dot{n}_j}{dz} \tag{61}$$

Note that here the physical equilibrium equality constraint is differentiated with respect to temperature, pressure and number of moles. Additional equations required for closure include a slip ratio or void fraction correlation, an equation of state valid for both phases and a frictional pressure drop correlation. One specified, equations (49) through (61) are then easily solved numerically.

For multicomponent single phase flow, say vapor, equations (49) through (61) can be simplified. The equations are solved explicitly for T, P, ρ, and u:

$$\frac{d\rho}{dz} = -\frac{\rho_v[E_0R_n + E_0M_0R_1 - E_1M_0R_0 + E_3R_0]}{D_1} \tag{62}$$

$$\frac{dP}{dz} = -\frac{E_0\rho_v R_n u^2 + E_3R_0\rho_v u^2 - E_2M_0R_0 u + E_0M_0\rho_v}{D_1} \tag{63}$$

$$\frac{dT}{dz} = \frac{E_1\rho_v R_n u^2 + E_3R_1\rho_v u^2 - E_2R_n u - E_2M_0R_1 u + E_1M_0\rho_v - E_3\rho}{D_1} \tag{64}$$

$$\frac{du}{dz} = \frac{u[E_0R_n + E_0M_0R_1 - E_1M_0R_0 + E_3R_0]}{D_1} \tag{65}$$

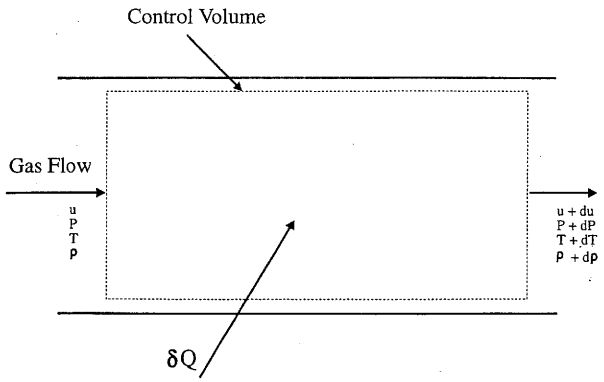

FIGURE 22. Flow of a gas with heat interaction.

where R_0, R_1, R_n, E_0, E_1, and E_n are constants defined earlier. E_2, E_3, D_1, and M_0 are constants defined by the following equations:

$$E_2 = u\dot{M} \tag{66}$$

$$E_3 = \frac{d\dot{Q}}{dz} - \frac{d\dot{W}}{dz} - E_n - \dot{M}g\sin\theta \tag{67}$$

$$D_1 = E_0R_1\rho_v u^2 - E_1R_0\rho_v u^2 + E_2R_0u - E_0\rho \tag{68}$$

$$M_0 = -\rho g\sin\theta - \left[\frac{dP}{dz}\right]_F \tag{69}$$

Before we examine issues related to reacting two-phase flow in pipes and their impact on pressure relief design, we analyze the simple case of an ideal gas flowing in a constant cross-sectional area pipe without friction. Heat is added to the flowing gas as shown in the control volume displayed in Figure 22. The state of the flowing gas can be described using the conservation of mass, momentum and energy:

$$\frac{d\rho}{\rho} + \frac{du}{u} = 0 \quad \text{or} \quad \rho u = \text{Constant} \tag{70}$$

$$dP + \rho u du = 0 \quad \text{or} \quad P + \rho u^2 = \text{Constant} \tag{71}$$

$$\delta Q = dH + udu \quad \text{or} \quad \frac{\delta Q}{du} = C_p\frac{dT}{du} + u \tag{72}$$

where δQ is the heat interaction per unit mass. The term dT/du in the energy equation can be expressed as a function of u and T. The ideal gas equation of state is first differentiated to yield:

$$\frac{dP}{P} = \frac{dP}{\rho R_g T} = \frac{dT}{T} + \frac{d\rho}{\rho} \tag{73}$$

We then replace $d\rho/\rho$ by $-du/u$ (from the continuity equation) and dP/ρ by $-udu$ (from the momentum equation) to yield:

$$\frac{dT}{du} = \frac{T}{u} - \frac{u}{R_g} \tag{74}$$

This equation indicates that dT/du is positive for small values of u and negative for large values of u. Substitution of this expression for dT/du in the energy equation leads to:

$$\frac{\delta Q}{du} = C_p\left(\frac{T}{u} - \frac{u}{R_g}\right) + u = C_p\frac{T}{u} - \frac{u}{\gamma - 1} \tag{75}$$

This relation shows that positive heat addition to the flowing gas will accelerate the flow when the velocity is small and will decelerate the flow when the velocity is large. When $\delta Q/du$ equals zero, the velocity equals the speed of sound:

$$\frac{\delta Q}{du} = 0 \quad \text{or} \quad u = \sqrt{\gamma R_g T} \tag{76}$$

We conclude from this simple exercise that for subsonic flow, positive heat interaction can either increase of decrease the fluid velocity. The positive heat interaction can be induced by heat transfer through the pipe walls, condensation of liquid droplets, chemical reaction, etc. In addition the following observations can be inferred (see Foa and Rudinger [*42*]):

- Both the flow conditions upstream and downstream from the heat interaction zone are modified,
- The velocity of the heated fluid does not necessarily increase to the sonic value when heat is added; it will increase or decrease depending on the boundary conditions,
- The mass flow rate may decrease as a result of the addition of heat; this decrease is not related to the attainment of sonic velocity in the heated region.

These conclusions have an impact on pressure relief design for two-phase systems where piping connects a reactor vessel to a separator or a vent containment system. Similar conclusions can be shown to exist in reacting two-phase flow in pipes (see Friz and Duffield [*43*]). For two-phase systems, the rate of heat generation as well as the rate of gas generation will influence the flow conditions. For example, a gassy reaction which adds mass to the gas phase with no significant heat evolution will force the flow to accelerate. Other variables such as void fraction, expansion cooling, friction heating, composition, etc. will influence the extent to which the flow conditions are affected.

In order to illustrate the impact of all these variables on reacting two-phase flow conditions, we examine a mixture containing hydrogen peroxide, water, and oxygen with mass fractions of 0.499, 0.499, and 0.0020, respectively. This mixture is flowing in a pipe (homogeneous-equilibrium flow, no slip) with a diameter equal to 6 inches. The stream void fraction is 0.013. Hydrogen peroxide decomposes in the liquid phase and forms oxygen and water according to the following stoichiometry:

$$H_2O_2 \rightarrow \frac{1}{2}O_2 + H_2O \tag{77}$$

The reaction is first order and has a temperature dependent rate described by the following expression:

$$K = 1.5\times10^{12}\exp\left(-\frac{12{,}832}{T}\right) \tag{78}$$

where K is in s^{-1} and T is in Kelvins.

Figure 23 illustrates the impact of reaction and varying inlet temperature and pressure conditions on maximum flow as a function of pipe length for two cases as follows:

1. High temperature/pressure inlet at 404 K and 5 bars.
2. Low temperature/pressure inlet at 345 K and 3 bars.

As shown by Figure 23, a continuing reaction in a pipe induces a highly nonlinear effect on pressure, temperature and composition. There is a competing effect between expansion cooling, friction, reaction heating and mass transfer between the liquid and the vapor phases. The magnitude of this effect depends on the inlet void fraction, temperature, pressure, pipe

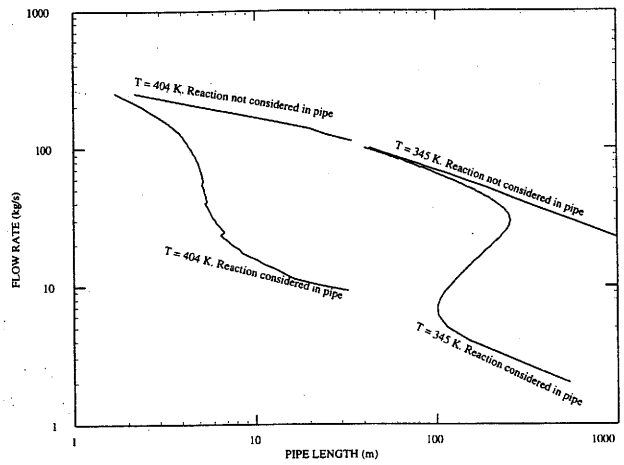

FIGURE 23. Maximum mass flow as a function of pipe length for reacting systems.

diameter, pipe roughness, etc. Figure 23 shows an S shaped curve which represents this competing effect. The S shaped curve is more pronounced for the lower pressure/temperature inlet conditions. Both S shaped curves indicate that the effect of continuing reaction in pipes can lead to multiplicity of steady states (i.e. a higher flow rate can be achieved with a shorter pipe) and/or a severe reduction in mass flow. This reduction in mass flow should be anticipated and accounted for in pressure relief design, especially when long pipes (long residence time) are present. To understand the impact of mass flow reduction on vessel pressure and temperature behavior we will use the same hydrogen peroxide data presented above. The vessel in question has a 50/50 hydrogen peroxide mixture and has an initial pressure of 1 bar and an initial temperature of 282 K. The vessel is exposed to an external fire with a flux of 75 kW/m^2. The vessel is equipped with a rupture disk set at 3 bars. Two cases are considered:

1. Rupture disk diameter is 3 inches with a 10 m horizontal pipe attached.
2. Rupture disk diameter is 4 inches with a 20 m horizontal pipe attached.

In both cases, the attached piping is insulated, i.e. no heat transfer from fire. Homogeneous equilibrium two-phase flow is assumed to occur for both cases. Figure 24 illustrates the impact of continuing reaction in the pipe on vessel pressure. The top curve is estimated accounting for reaction effects in the pipe. The bottom curve is estimated without reaction effects in the pipe. The difference is substantial.

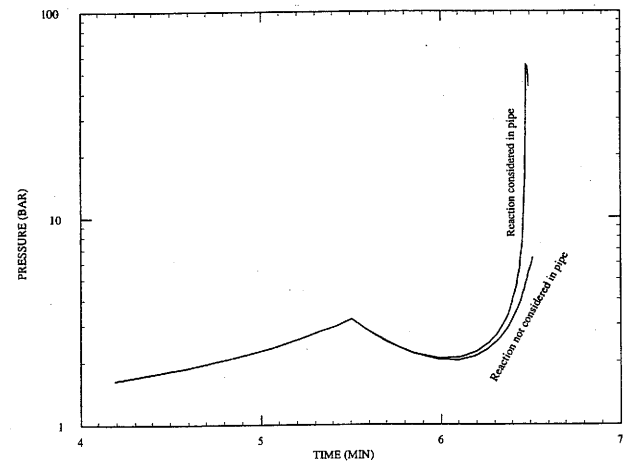

FIGURE 24. Vessel pressure history for case 1. 3-inch rupture disk with a 10 m horizontal pipe.

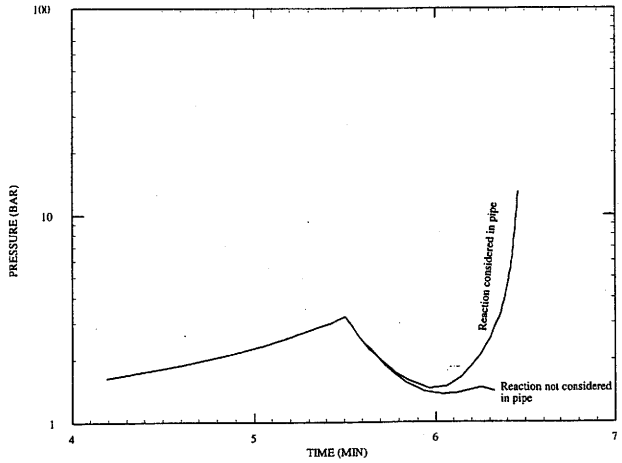

FIGURE 25. Vessel pressure history for case 2. 4-inch rupture disk with a 20 m horizontal pipe.

Figure 25 illustrates the impact of continuing reaction on vessel pressure for case 2. The difference is more pronounced due to the presence of a longer pipe with a larger diameter.

REACTIVITY TESTING GUIDELINES

A variety of techniques are used commercially for evaluation of the essential parameters identified above. We consider that use of a combination of approaches and techniques is essential to identify and quantify the necessary parameters with confidence and to highlight any specific system or instrument characteristics which might influence a particular evaluation. No single instrument or technique is likely to give the full range of required information for the majority of reactive systems of interest. For example, under a constant volume environment, some reactions produce volatiles which could remain in the liquid phase and inhibit other potentially dangerous liquid phase reations. By the same token, for an open system test, a reaction might not reach a pressure level that is required for another reaction to propagate or for a critical energy density. There are such systems where detonations have been observed at or above certain critical pressure levels.

In view of the above, we propose to utilize a combination of theoretical, experimental and numerical techniques in our evaluation of relief system design. This would typically include (but may not necessarily be limited to) the following:

1. Thermochemical Evaluation, heat of formation data, oxygen balance.
2. Reactivity Screening, e.g. Differential Scanning Calorimeter (DSC), Reactive System Screening Tool (RSST).
3. Kinetic Evaluation, e.g. Accelerating Rate Calorimeter (ARC) or other adiabatic calorimetric methods.
4. Pressure Rate Evaluation, e.g. ARC, VSP testing (closed), analysis of collected decomposition products by gas chromatography to elucidate reaction mechanisms.
5. Scaleup, to take account of mechanisms for heat transfer between the full-scale industrial reactor and its environment during normal and transient operating conditions (e.g. external fire).
6. Vent System Design, using the above derived data to predict the pressure and temperature histories of the full-scale plant under runaway conditions, in conjunction with our advanced predictive multicomponent, multiphase flow models and state of the art numerical analysis techniques.

Numerical methods and software analysis techniques for the above have been developed to the extent that rapid interactive analysis of system data is possible. This readily facilitates vent

Table 7 Summary of Reactivity Testing and Relief System Design Strategy

Evaluation Stage	Methodology	Output Data: Thermal Stability	Heat of Reaction	Global Kinetic Data	Gas Generation Data	System Characteristics	ERS Device
Thermochemical Evaluation	CHETAH		×				
	Heats of Formation		×				
	Oxygen Balance	×					
Reactivity Screening	DSC	×	×				
	RSST	×					
Kinetic Evaluation	ARC		×	×			
Pressure Rate Evaluation	ARC				×		
	VSP (Closed)				×		
Scaleup	System Parameters					×	
	Design Codes					×	
ERS System	Design Optimization						×

design optimization in terms of relief set pressure, maximum vessel internal pressure rise and relief venting rate.

TESTING STRATEGY

We propose the following testing strategy as summarized in Table 7:

1. Thermochemical Evaluation: Heat of reaction can be estimated from standard heats of formation of the reactants and most stable decomposition products as a bounding case. Where heat of formation data are not available for more obscure/exotic components, these can be estimated from standard heats of combustion in conjunction with heat of formation of predicted combustion products (typically carbon dioxide and water). Bond energy and group contribution methods can also be utilized for determination of heat of reaction. An oxygen balance can be indicative of potential inherent instability.
2. Reactivity Screening: Both DSC and RSST provide means of determining system reactivity during programmed heating through a specified temperature range. Where the sample is sufficiently homogeneous to provide a representative sample on a small-scale, sealed capsule DSC provides a highly accurate measurement of reaction heat.
3. Kinetic Evaluation: The ARC is particularly well suited to global kinetic characterization due to its sensitivity and high relative adiabaticity. Although much emphasis has been placed by manufacturers on the thermal inertia or phi-factor, an instruments' ability to track an exotherm in order to maintain pseudo adiabatic conditions and quantify heat transfer within the sample's local environment is equally important if meaningful kinetic data are to be obtained.
4. Pressure Rate Evaluation: Pressure rate evaluation should use a combination of data from the ARC and/or VSP (closed), together with gas chromatography of reaction products, where appropriate.
5. Scaleup: Scaleup should take account of size, configuration and operating conditions of a full-scale plant. In particular, the extent of mixing, natural cooling losses and forced cooling capacity of the vessel should be considered. The effect of vessel wall conductivity, external insulation and external jacket structures should be considered, where appropriate.
6. Vent System Design: Derived data can be used to predict the transient temperature and pressure vs. time behavior of the full-scale plant under runaway conditions for events initiated by intrinsic maloperation or by external fire loading. The analysis should take due account of any existing mitigating measures and should make recommendations for any additional protective measures which become apparent from the analysis.

We recommend that consideration be given in the test procedures to the effects of impurities or contaminants on the thermal stability or reactivity of test materials. Typically this might include water, materials of construction and their corrosion products, abnormal concentrations of by-products, and packaging materials. In some cases, normal contact with structural materials may catalyze exothermic reactions. It is also important to note that contaminants can also inhibit the reaction rates in the early stages of a runaway or decomposition. This can lead to accumulation of chemical energy which is released once unstable conditions are reached.

The effects of scaleup, i.e. thermal inertia, vapor-liquid disengagement, nonequilibrium flashing flow, and external heating on vent sizing should be carefully evaluated.

CONCLUSIONS

This paper presents a detailed framework for pressure relief design for single-phase and two-phase reacting multicomponent system and proposes a general reactivity testing strategy.

A new method is developed for identifying reaction stoichiometry, chemical identity for reaction products and reaction rates from closed volume test data. The number of species considered is currently limited to a database of 1300 chemicals. Work is nearing completion on a variation of this scheme which will use group contribution concepts to generate all possible chemical structural permutations for reaction products.

In addition, the detailed approach outlined in this paper considers vessel failure mechanisms and inherent stability limits on relief system temperature and depressurization rates as well as the impact of continuing reaction in piping on mass flow reduction.

NOTATION

A = area (m^2)
A_E = available energy (J/kg)

C = concentration (volume percent)
C_d = discharge coefficient
C_p = heat capacity at constant pressure (J/kmol/K)
C_v = heat capacity at constant volume (J/kmol/K)
d = diameter (m)
E = efficiency; activation energy (J/kmol)
f = fanning friction factor
g = acceleration due to gravity (9.8 m/s^2)
G = Gibbs free energy (J); mass flux (kg/m^2/s)
h = heat transfer coefficient (J/s/m^2/K)
H = enthalpy (J)
k = reaction rate
K = equilibrium constant; mass transfer coefficient
m = liquid mass (kg)
M = mass; vapor mass (kg)
M_w = molecular weight (kmol/kg)
n = liquid number of moles (kmol)
N = number of moles; vapor number of moles (kmol)
P = pressure (Pa)
q = heat per unit area (J/m^2)
Q = heat (J)
R_g = universal gas constant, 8314 (J/kmol/K)
S = entropy (J/K)
t = time (s)
T = temperature (K)
u = velocity (m/s)
U = internal energy (J)
V = volume (m^3)
v = specific volume (m^3/kg)
x = horizontal distance; downwind distance (m)
X = liquid mole fraction
Y = vapor mole fraction
z = vertical distance; height; elevation; depth (m)
Z = compressibility factor

Subscripts

c = critical, centerline
C = chemical; combustion
f = friction; final; flame; forward
g = gas
h = hole; orifice
i = inside; inner
in = input
l = liquid
m = mixture
0 = initial; reference
o = outside; outer
out = output
r = reduced
s = surrounding medium
sat = saturated
T = total
v = vapor
vl = vapor-liquid interface
w = water; wetted
x = molar (/kmol)
x = x direction; x component
y = y direction; y component
z = z direction; z component

Superscripts

$\dot{x}$ = rate, x units/s
$\bar{x}$ = partial molar; time averaged; average
$\hat{x}$ = nonideal

Greek

β = volume expansivity (/K)
ρ = density (kg/m^3)
ν = kinematic viscosity (m^2/s)
μ = viscosity (kg/m/s); chemical potential
α = thermal diffusivity (m^2/s); void fraction
λ = latent heat of vaporization (J)
π = 3.141592654
γ = heat capacity ratio (C_p/C_v)
Φ = fugacity coefficient; thermal inertia
θ = angle with respect to horizontal
κ = isothermal compressibility (/Pa)
Δ = difference

LITERATURE CITED

1. **Nolan, P. F., N. R. Hardy, and G. N. Pettitt**, "The Physical Modeling of Two-Phase Releases Following the Sudden Failure of Pressurized Vessels," in *International Conference and Workshop on Modeling and Mitigating the Consequences of Accidental Releases of Hazardous Materials*, pp. 125–143, CCPS, AIChE (1991).
2. **Bettis, R. J., G. M. Makhviladze, and P. F. Nolan**, "Expansion and Evolution of Heavy Gas and Particulate Clouds," *Journal of Hazardous Materials*, **14**, 213–233 (1987).
3. SFPE, *Handbook of Fire Protection Engineering*, NFPA (1988).
4. **Prugh, R. W.**, Quantitative Evaluation of BLEVE Hazards," *J. of Fire Prot. Engr.*, **3**(1), 9–24 (1991).
5. **Leslie, I. R. M., and A. M. Birk**, "State of the Art Review of Pressure Liquefied Gas Container Failure Modes and Associated Projectile Hazards," *Journal of Hazardous Materials*, **28**, 329–365 (1991).
6. **Roberts, A. F., D. P. Cutler, and K. Billinge**, "Fire Engulfment Trials with LPG Tanks with a Range of Fire Protection Methods," in *4th International Symposium on Loss Prevention and Safety Promotion in the Process Industries*, pages D1–D10, Inst. Chem. Eng. Symp. Series No. 82, Pergamon, Manchester (1983).
7. **Moodie, K., L. T. Cowley, R. B. Denny, L. M. Small, and I. Williams**, "Fire Engulfment Tests on a 5 Tonne LPG Tank," *Journal of Hazardous Materials*, **20**, 55–71 (1988).
8. **Droste, B., and W. Schoen**, "Full-Scale Fire Tests with Unprotected and Thermal Insulated LPG Storage Tanks," *Journal of Hazardous Materials*, **20**, 41–53 (1988).
9. **Schoen, W., and B. Droste**, "Investigation of Water Spraying System for LPG Storage Tanks by Full-Scale Fire Tests," *Journal of Hazardous Materials*, **20**, 73–82 (1988).
10. **Reid, R. C.**, "Possible Mechanism for Pressurized-Liquid Tank Explosion or BLEVEs," *Science*, **203**, 1263–1265 (1979).
11. **Jones, M. R.**, "Vapour Explosions Resulting from Rapid Depressurization of Liquids: the Importance of Initial Temperature," in *Inst. Chem. Eng. Symp. Series 93*, pp. 357–362, Inst. of Chem. Eng., Pergamon (1985).
12. **Martinsen, W. E., D. W. Johnson, and W. F. Terrel**, "BLEVEs: Their Causes, Effects, and Prevention," *Hydrocarbon Processing*, **5**(11), 141–148 (1986).
13. **Davenport, J. A.**, "Hazards and Protection of Pressure Storage and Transportation of LP Gas," *Journal of Hazardous Materials*, **20**, 3–19 (1988).
14. **Dunn, V.**, "BLEVE: The Propane Cylinder," *Fire Engineering*, **131**, 63–70 (1988).
15. **Beegle, B. L., M. Modell, and R. C. Reid**, "Thermodynamic Stability Criterion for Pure Substances and Mixtures," *AIChE Journal*, **20**(6), 1200–1206 (1974).

16. **Heidemann, R. A.**, "The Criteria for Thermodynamic Stability," *AIChE Journal*, **21**(4), 824–826 (1975).
17. **W. M. Porteous and R. C. Reid**, "Light Hydrocarbon Vapor Explosions," *Chemical Engineering Progress*, 83–89 (1976).
18. **Melhem, G. A., P. A. Croce, and H. Abraham**, "Data Summary and Analysis of NFPA's BLEVE Tests," in *26th Annual Loss Prevention Symposium*, pp. 1–19, Safety and Health Division, AIChE (1992).
19. **Birk, A. M., M. Cunningham, Z. Ye, and J. Maillette**, "Medium-Scale Fire Tests Investigating a BLEVE Event," in *Tenth Technical Seminar on Chemical Spills*, pp. 203–220, Environment Canada (1993).
20. **Ogiso, C., N. Takagi, and T. Kitagawa**, "On the Mechanism of Vapor Explosion," in *Loss Prevention and Safety 9*, pp. 233–240, PACHEC (1972).
21. **Venart, J. E. S.**, "To BLEVE or not to BLEVE: Anatomy of a Boiling Liquid Expanding Vapor Explosion," Fire Science Centre, University of New Brunswick, Canada (1991).
22. **Fujikawa, S., and T. Akamatsu**, "Effects of the Non-Equilibrium Condensation of Vapour on the Pressure Wave Produced by the Collapse of a Bubble in a Liquid," *J. Fluid Mech.*, **97**(3), 481–512 (1980).
23. **Elias, E., and P. L. Chambre**, "Flashing Inception in Water During Rapid Decompression," *Journal of Heat Transfer*, **115**, 231–238 (1993).
24. NFPA 30, *Flammable and Combustible Liquids Code* (1993).
25. NFPA 15, *Water Spray Fixed Systems for Fire Protection* (1990).
26. API 520, *Sizing, Selection and Installation of Pressure-Relieving Devices in Refiners. Part 1—Sizing and Selection*, 6th ed. (1993).
27. **Fisher, H. G.**, "DIERS Research Program on Emergency Relief Systems," *Chemical Engineering Progress*, **81**(8), 33–36 (1985).
28. **Grolmes, M. A., and Leung, J. C.**, "Code Method for Evaluating Integrated Relief Phenomena," *Chemical Engineering Progress*, **81**(8), 47–52 (1985).
29. **Shaw, D. A.**, "SAFIRE Program for Design of Emergency Pressure Relief Systems," *Chemical Engineering Progress*, **86**(7), 14–17 (1990).
30. **Fisher, H. G.**, "An Overview of Emergency Relief System Design Practice," *Plant/Operations Progress*, **10**(1), 1–12 (1991).
31. DIERS, "Technology Summary—Emergency Relief System for Runaway Chemical Reactions and Storage Vessels: A Summary of Multiphase Flow Methods," Technical Report FAI/83-27, AIChE (1986).
32. **Fisher, H. G., *et al.***, "Emergency Relief System Design Using DIERS Technology," *The DIERS Project Manual*, AIChE/DIERS (1992).
33. ASME, "ASME Boiler and Pressure Vessel Code," Section VIII, Rules for Construction of Pressure Vessels (1992).
34. **Leung, J. C., H. K. Fauske, and H. G. Fisher**, "Thermal Runaway Reactions in a Low Thermal Inertia Apparatus," *Thermochim. Acta.*, **104**, 13–29 (1986).
35. **Leung, J. C., M. J. Creed, and H. G. Fisher**, "Round-Robin Vent Sizing Package Results," in *International Symposium on Runaway Reactions*, CCPS/AIChE (1989).
36. **Fauske, H. K., G. H. Clare, and M. J. Creed**, "Laboratory Tool for Characterizing Chemical Systems," in *International Symposium on Runaway Reactions*, CCPS/AIChE (1989).
37. **Michelsen, M. L.**, "An Efficient General Purpose Method for the Integration of Stiff Ordinary Differential Equataions," *AIChE Journal*, **22**(3), 594–597 (1976).
38. **Townsend, D. I.**, "Accelerating Note Calorimetry," *Chem. Eng. Prog.*, **73**, 80 (1977).
39. **Townsend, D. I., and J. C. Tou**, "Thermal Hazard Evaluation by An Accelerating Rate Calorimeter," *Thermochim. Acta.*, **37**, 1 (1980).
40. **Melhem, G. A., R. Saini, and B. M. Goodwin**, "A Modified Peng-Robinson Equation of State," *Fluid Phase Equilibria*, **47**, 189–237 (1989).
41. **Hougen, O. A., and K. M. Watson**, *Chemical Process Principles. Part I, Material and Energy Balances*, Wiley (1946).
42. **Foa, J., and G. Rudinger**, "On the Addition of Heat to a Gas Flowing in a Pipe at Subsonic Speed," *Journal of the Aeronautical Sciences*, **16**(2), 84–94 (1949).
43. **Friz, G., and J. S. Duffield**, "Critical Flow of a Chemically Reacting Two-Phase Multicomponent Mixture in a Tube," in *26th European Two-Phase Flow Group*, Commission of the European Communities, JRC-Ispra (1991).

This paper (9b) was presented at the AIChE Spring National Meeting in Atlanta, GA on April 18, 1994.